Journal of Integrative Agriculture 2026, 25(9): 3639–3655

KeAi CHINESE ROOTS GLOBAL IMPACT

Available online at ScienceDirect

Journal of Integrative Agriculture

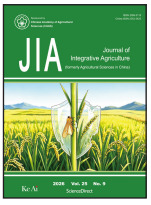

RESEARCH ARTICLE

Exogenous prohexadione-calcium enhances soybean yield under saline–alkali stress by modulating ion homeostasis, ascorbate–glutathione defense, and photosynthesis

Minglong Yu[1, 2*], Lu Huang[1, 3*], Aaqil Khan[1], Naijie Feng[1, 4], Dianfeng Zheng[1, 4#]

[1] *College of Coastal Agriculture Sciences, Guangdong Ocean University, Zhanjiang 524088, China*
[2] *College of Agronomy and Biotechnology, China Agricultural University, Beijing 100194, China*
[3] *College of Horticulture, Hunan Agricultural University, Changsha 410128, China*
[4] *Shenzhen Research Institute, Guangdong Ocean University, Shenzhen 518108, China*

Highlights

- Prohexadione-calcium (Pro-Ca) application increased soybean yield under saline–alkali stress by inhibiting Na^+ influx, activating the ascorbate–glutathione cycle, and maintaining biomembrane systems.
- Pro-Ca application inhibited the degradation of chlorophyll and also protected the ultrastructural stability of chloroplasts.
- 100 mg L^{-1} Pro-Ca can be used as a suitable concentration for spraying soybeans in saline–alkali soil.

Abstract

Prohexadione-calcium (Pro-Ca) has been shown to positively regulate crop tolerance to saline–alkali stress. However, the optimal concentration of Pro-Ca application and the mechanisms through which it enhances saline–alkali tolerance and yield in soybean remain unclear. This study aimed to determine the optimal concentration of exogenously applied Pro-Ca and reveal the mechanisms underlying Pro-Ca's effect on remediation and yield response in soybean under saline–alkali stress. The results indicated that saline–alkali stress negatively impacted the morphological and physiological traits of soybean seedlings by triggering the production of reactive oxygen species (ROS), leading to oxidative damage of the grana lamellae due to excessive accumulation of Na^+. An application of 100 mg L^{-1} Pro-Ca was found to be optimal, promoting dry matter accumulation and normalized difference vegetation index (NDVI) by significantly reducing Na^+ uptake under saline–alkali stress. Moreover, integrated physiological, ultrastructural, and transcriptomic analyses indicated that Pro-Ca significantly enhanced the ascorbate–glutathione (AsA–GSH) cycle by up-regulating the expression of related genes to enhance the activities of ascorbate peroxidase (APX), glutathione reductase (GR), dehydroascorbate reductase (DHAR), monodehydroascorbate reductase (MDHAR), and the AsA/dehydroascorbate (DHA) and GSH/oxidized glutathione (GSSG) ratios to quench ROS, thereby protecting both thylakoid and mitochondrial membranes from degradation. The differentially expressed genes (DEGs) encoding ascorbate and aldarate metabolism were significantly (P<0.05) enriched in the integral component of the membranes. Furthermore, Pro-Ca treatment up-regulated the expression of genes encoding photosystems under saline–alkali stress, thereby reducing the photoinhibition and stomatal limitation (L_s), mitigating damage to photosystems, and preventing yield reduction. In summary, foliar application of Pro-Ca could efficiently enhance soybean seedlings' tolerance to saline–alkali stress by inhibiting Na^+ influx, enhancing the AsA–GSH cycle, maintaining the biomembrane system, and improving photosynthetic efficiency.

Keywords: soybean, prohexadione-calcium, saline–alkali stress, physiological, ultrastructural, transcriptomic

Received 8 December 2024; Received in revised form 13 February 2025; Accepted 3 March 2025; Available online 3 April 2025
Minglong Yu, E-mail: 15776559827@163.com; #Correspondence Dianfeng Zheng, E-mail: zhengdf@gdou.edu.cn
* These authors contributed equally to this study.

doi: 10.1016/j.jia.2025.04.005

1. Introduction

Soybean (*Glycine max* L.) is a vital oilseed crop, as it possesses 40% protein and 20% oil content (Duan *et al.* 2024). Globally, around 60% of edible oil production and 70% of plant protein are consumed by humans and animals (Akram *et al.* 2017). It is estimated that approximately 20% of the world's arable land and 33% of irrigated croplands are subjected to soil salinization (Alam *et al.* 2019; Hassani *et al.* 2021). The salt-infested area in China is about 9.2×10^7 ha, equivalent to 5% of the total land area (Zhang *et al.* 2019). The main sources of soil salinization are climate change due to global warming, rising sea levels, overuse of fertilizers and pesticides, and poor land and water management practices (Hassani *et al.* 2021). Excessive Na^+ and Cl^- ions in saline and alkaline soils disrupt many physiological and biochemical processes that impair plant growth and productivity (Zhang *et al.* 2023). Soybean is classified as a moderately salt-sensitive crop (Estaji and Niknam 2020; Zhang *et al.* 2023). Soybean cultivation in agricultural production systems must cope with these challenges caused by saline–alkali stress (Mehmood *et al.* 2020). There is an urgent need for new production strategies, such as cultivation techniques and soybean salt-resistive varieties approach, to improve soybean productivity and ensure food security (Peña-Calzada *et al.* 2023). Therefore, enhancing soybean saline–alkaline tolerance and alleviating stress-induced damage would enable more effective use of salinized soil.

Saline–alkali stress disrupts metabolic processes, including physiological, transcriptional, and cellular approaches, leading to plant growth retardation (Peña-Calzada *et al.* 2023). Oxidative stress caused by overproduction of reactive oxygen species (ROS) produces toxic effects (Sharma *et al.* 2016; Waszczak *et al.* 2018; Mittler *et al.* 2022). In photosynthetic systems, insufficient energy dissipation results in O_2 receiving electrons from the reducing side of photosystem I (PSI) that leakage occurs by overloading the electron transport chain (ETC) and using the excess photon energy to form superoxide radicals ($O_2^{-}\cdot$) *via* the Miller reaction (Mehler 1951; Zhao *et al.* 2023). Subsequently, $O_2^{-}\cdot$ can be disproportionate to H_2O_2 by superoxide dismutase (SOD) inside the thylakoid (Zhang *et al.* 2021). Excessive accumulation of ROS ($O_2^{-}\cdot$ and H_2O_2) under saline–alkali stress causes photo oxidative damage to PSII (Deng R *et al.* 2024). The recovery rate of PSII is lower than the rate of damage, due to its inhibition activity, which in turn disrupts the structure of the thylakoid membrane, leading to a reduction in transcription levels of photosynthesis-related genes such as *Lhca*, *PsaA*, *PsaB*, *PsbA*, *PsbC*, and *Cytb6f*, which in turn decreases electron transport efficiency and photosynthetic performance (Gupta *et al.* 2017). Additionally, ROS can be generated in mitochondria, plasma membranes, and endoplasmic reticulum, leading to energy production chain breakage, lipid and protein damage (Rasool *et al.* 2013; Zhao *et al.* 2023). To adapt to such stressful environments, plants have evolved various adaptive mechanisms to maintain cellular ionic homeostasis and a strong antioxidant defense system to quench bursts of ROS (Du *et al.* 2024). Especially, the Na/H anti-transporter SOS1, located at the plasma membrane, can induce Na^+ exclusion from roots using a proton gradient generated by H-ATPase, whereas initiation of NHX1 signaling at the tonoplast enables the driving of Na^+ segregation into vacuoles (Sun *et al.* 2019). This is a major effective strategy for plants to mitigate Na^+ toxicity to maintain cellular ion homeostasis (Gadelha *et al.* 2021). Most importantly, the ascorbate–glutathione (AsA–GSH) cycle functions mainly in the cytoplasm, mitochondria, plastids, and peroxisomes, ultimately reducing toxic H_2O_2 to H_2O through the efficient turnover of four key enzymes, i.e., ascorbate peroxidase (APX), monodehydroascorbate reductase (MDHAR), dehydroascorbate reductase (DHAR), and glutathione reductase (GR), and two antioxidants (AsA and GSH), to maintain cellular redox homeostasis and attenuate the oxidative damage of ROS (Raja *et al.* 2017). Therefore, the AsA–GSH cycle plays a central role in plant antioxidant defense responses, and researchers can evaluate the plant resistance to saline–alkali stress by monitoring antioxidant capacity (Hasanuzzaman *et al.* 2019). However, these defense mechanisms may be weakened by changes in the intensity of the stress, both in time and concentration. Therefore, applying new interventions to plants exposed to saline–alkali stress to increase their stress tolerance would be a positive achievement. In recent years, the use of plant growth regulators as a strategy to enhance plant response to saline–alkali stress has received widespread consideration (Gupta *et al.* 2017).

Prohexadione-calcium (Pro-Ca) is a plant growth retardant that inhibits gibberellin synthesis by inhibiting the 3,β-hydroxylation of GA_{20} to GA_1 (Nakayama *et al.* 1990). Several recent studies have demonstrated the positive role of Pro-Ca in mitigating abiotic stresses in plants (Li *et al.* 2023). Exogenous Pro-Ca enhances photosystem efficiency in soybean (Feng *et al.* 2021) and *Vicia faba* under saline–alkali stress by increasing antioxidant enzyme activities to detoxify ROS (Bekheta *et al.* 2009). Pro-Ca treatment inhibited the activities of phospholipase D and lipoxygenase, maintaining lower levels of malondialdehyde (MDA) in tomato exposed to chilling injury (Aghdam 2013). Moreover, the function of Pro-Ca has been demonstrated in the transcriptome, implying that it supports rice to cope with salt stress by up-regulating the metabolite network of genes related to photosynthesis and chlorophyll synthesis while maintaining a low Na^+/K^+ ratio (Li *et al.* 2023).

Previous studies demonstrated the structural, physiological, and molecular mechanisms of exogenous application of Pro-Ca for adaptation to saline–alkali stress in soybean, especially the dosage management of Pro-Ca for foliar spraying. Further investigations required to understand the potential mechanisms and optimal strategies for the application of Pro-Ca in soybean plants under saline–alkali stress. Therefore, the current study investigated the critical expression pathways of the soybean transcriptome under saline–alkali stress induced by exogenous spraying of Pro-Ca using the salt-sensitive soybean cultivar Kenfeng 16 and verified this hypothesis in conjunction with photosynthetic fluorescence response, AsA–GSH cycle, ion homeostasis, ultrastructure, and expression of related genes. This study further elucidated the underlying mechanisms and effective

application doses of Pro-Ca in response to saline–alkali stress in soybean and provided a theoretical basis for the application of Pro-Ca in soybean production in saline–alkali soil.

2. Materials and methods

2.1. Plant materials

The plant material soybean cultivar Kenfeng 16 and the plant growth regulator Pro-Ca were obtained from the Chemical Control Group of the Agricultural College of Heilongjiang Bayi Agricultural University, China. Uniform and mature seeds were selected and sterilized for 2 min with 5% NaClO, and then rinsed three times with distilled water to remove the attached chloride. Subsequently, 10 seeds were randomly selected and sown in plastic pots containing 1 kg of soil (garden soil:vermiculite=1:2, containing 91.2 mg kg^{-1} of alkali-hydrolyzable nitrogen, 41.5 mg kg^{-1} of available phosphorus, 123.2 mg kg^{-1} of available potassium, 25.4 g kg^{-1} of organic matter, and pH was 6.61). The seedlings were then transferred to a solar greenhouse to be grown under natural light conditions with day/night temperatures of 26°C/22°C, day/night photoperiods of 10/14 h, and relative humidity of 60/70%. Eight well-grown seedlings were retained in each pot after emergence.

2.2. Treatments with saline–alkali and Pro-Ca

Experiment 1: For further treatments, seedlings with the same water management up to the fully developed third trifoliate leaf (V3) stage were randomly divided into two groups. In the first group, seedlings were exposed to 110 mmol L^{-1} saline–alkali solution, both alone and in combination with different concentrations of Pro-Ca (0, 5, 25, 50, 100, and 200 mg L^{-1}) as co-treatment for 15 days. The Pro-Ca solution was sprayed with a hand sprayer, ensuring that each leaf was completely drenched. Soil saline–alkali concentration was maintained by monitoring soil conductivity using a plug-in conductivity meter (ECTestr11+, USA). 100 mg L^{-1} Pro-Ca was selected as the optimal dose from several trial experiments, and it conferred better performance under 110 mmol L^{-1} saline–alkali solution in soybean seedlings as measured by the dry weight per plant and net photosynthetic rate (P_n) responses. Our preliminary experiments and a previous study (Guo *et al.* 2015) indicated that 110 mmol L^{-1} saline–alkali solution ($NaCl:Na_2SO_4:NaHCO_3:Na_2CO_3$=9:1:9:1, pH=8.42±0.043) causes moderate stress in soybeans.

Experiment 2: In the second group, seedlings were divided into four treatments: CK (water+water without saline–alkali solution), Pro-Ca (100 mg L^{-1} Pro-Ca+water without saline–alkali solution), SA (water+water with saline–alkali solution), and SA+Pro-Ca (100 mg L^{-1} Pro-Ca+water with saline–alkali solution). A randomized block design with three biological replicates was used in this experiment. The first trifoliate leaves were collected from the plants 0, 3, 6, 9, 12, and 15 days after the initiation of Pro-Ca application for physiological analysis.

Experiment 3: The field experiment was conducted from May to September 2021 at the Jixiang Village Experimental Base in Lindian County, Daqing City, Heilongjiang Province, China. The 0–30 cm soil contained 133.48 mg kg^{-1} of alkali–hydrolyzable nitrogen, 12.67 mg kg^{-1} of available phosphorus, 216.53 mg kg^{-1} of available potassium, 31.57 g kg^{-1} of organic matter, and pH was 8.14. The experiment was conducted in a split-split plot design with three replications, with saline–alkali stress as the main factor and Pro-Ca as the sub-factor. The plot area was 19.5 m^2 (row spacing of 0.65 m, row length of 6 m, and 5-row of plot), and the seedling retention density was 220,000 plants ha^{-1}. Pro-Ca and saline–alkali treatments were performed at the R1 growth stage, with treatment settings consistent with experiment 2. Plants were sheltered to prevent rainfall, and salt was evenly sprayed using micro-spray belt irrigation to simulate saline–alkali stress. Fertilizers were applied in the form of basal application of 161.4 kg ha^{-1} of diammonium phosphate, 97.5 kg ha^{-1} of potassium sulphate and 71.1 kg ha^{-1} of urea.

2.3. Measurement of phenotypic parameters

Three soybean seedlings of equal growth were selected for each treatment and immersed in water to remove adherent soil. Phenotypic characteristics such as plant height, root length, shoot dry weight, and root dry weight were then investigated. The dry weight per plant included both shoot and root dry weight. Root/shoot ratio was calculated by the root dry weight divided by the shoot dry weight.

After 6 and 15 days of treatments, soybean plant seedlings were scanned using the Planteye F500 (Phenospex, Switzerland), a plant laser 3D phenotyping instrument, to measure and collect digital phenotypic data of the plants, including greenness (GI), normalized difference vegetation index (NDVI), leaf area index (LAI), Hue, and projected leaf area (PLA). 3D models of the plants were built using Phena software (Phenospex, Netherlands).

2.4. Transcriptome sequencing

Soybean leaves were collected 24 h after CK, SA, and SA+Pro-Ca treatments for RNA-seq analysis in three biological replicates. HiSeq (Illumina) preparation and sequencing of 9 mRNA libraries were outsourced to Biomarker Technologies (Beijing, China) based on the MGISEQ-2000 platform. Low-quality reads, adapters, and polyN sequences were removed from the raw data using fastp 0.21.0 to obtain clean reads. Differentially expressed genes (DEGs) between CK *vs*. SA and SA *vs*. SA+Pro-Ca treatments were identified using the DESeq 2 R package at $|\log_2 \text{fold change}| \geq 1.5$ and false discovery rate (FDR)<0.05. GO (Gene Ontology) and KEGG (Kyoto Encyclopedia of Genes and Genomes) enrichment analysis were performed using clusterProfile.

2.5. Measurement of Na^+, K^+, and chlorophyll content

At 15 days after treatment, 0.1 g of dried ground leaf samples were digested with HNO_3:$HClO_4$ (5:1; v/v) and Na^+ and K^+ contents were determined using atomic absorption spectrometry (PinAAcle 900H, Perkin Elmer) following the method of Sun *et al.* (2019). Chlorophyll *a* (Chl *a*), Chl *b*, carotenoids (Car), and total chlorophyll (Chl_{total}) were determined using the methods described by Alam *et al.* (2019).

2.6. Measurement of gas exchange parameters

The P_n and intercellular CO_2 concentration (C_i) of the fully expanded first trifoliate leaves were measured from 8:30 to 11:30 a.m. using a portable photosynthesis system, LI-6400XT (LI-COR, USA). The leaf chamber was set up under conditions of 1,000 μmol m^{-2} s^{-1} PAR, 400 ppm CO_2 concentration, and a leaf temperature of 26.0°C. Apparent mesophyll conductance (AMC) and stomatal limit (L_s) were calculated using the following formula (Xu *et al.* 2019; Xin *et al.* 2024):

$$AMC=\frac{P_n}{C_i}$$

$$L_s\ (\%)=\left(1-\frac{C_i}{C_a}\right)\times 100$$

where C_a is the ambient CO_2 concentration, i.e., the CO_2 concentration at the inlet of the instrument.

2.7. Measurement of chlorophyll fluorescence parameters

The same functional leaves as for the determination of gas exchange parameters were selected, and the fluorescence parameters of the leaves were determined by *OS5p* modulated chlorophyll fluorometer (OPTI-sciences, USA) at 9:00–11:30 a.m. at 6 and 15 days after treatment (Tang *et al.* 2021). The maximal photochemical efficiency of PSII (F_v/F_m), potential activity of PSII (F_v/F_o), electron transport rate (ETR), PSII actual photochemical quantum yield (Y(II)), maximal fluorescence (F_m), steady-state fluorescence (F_s), light-adapted maximum fluorescence yield (F_m'), and light-adapted minimal fluorescence (F_o') were recorded on a chlorophyll fluorometer by application of saturated light pulses to dark-adapted leaves after 30 min. The remaining fluorescence parameters were calculated according to the following equations: nonphotochemical quenching coefficient, $NPQ=(F_m-F_m')/F_m'$; photochemical quenching coefficient, $q_P=1-(F_s-F_o')/(F_m'-F_o')$; effective quantum yield of photochemical energy conversion in PSII, $\Phi PSII=(F_m'-F_s)/F_m'$.

At 15 days after treatment, leaves that had completed 30 min of dark adaptation were subjected to continuous illumination of 3,000 μmol m^{-2} s^{-1} red light using an OS5p modulated chlorophyll fluorometer. Instantaneous fluorescence was recorded from 10 μs to 300 s to generate the induced chlorophyll fluorescence kinetic curve (OJIP curve). JIP-test analysis of the obtained OJIP curves was performed according to the method of Stirbet and Govindjee (2011). The parameters are summarized in Appendix A.

2.8. Measurement of AsA–GSH cycle, sucrose, and starch content

The AsA, dehydroascorbate (DHA), GSH, and oxidized glutathione (GSSG) contents, as well as APX, GR, DHAR, and MDHAR activities, were quantified using the plant extraction kits (Solarbio, China) according to the manufacturer's protocol. The H_2O_2 and MDA contents were determined according to the method of Liu *et al.* (2024). The sucrose and starch contents were determined according to the anthrone method described by Estaji and Niknam (2020).

2.9. Leaf ultrastructure

At 15 days after treatment, 2 mm^2 leaf segments were cut, fixed with 2.5% glutaraldehyde (pH 7.5), and stored in a refrigerator at 4°C for 24 h. The samples were then rinsed three times with 0.1 mol L^{-1} phosphate buffer and fixed with 1.5% OsO_4 for 4 h. Subsequently, they were dehydrated with a gradient of ethanol and acetone for 15 min each, embedded in Epon812 epoxy resin, cured, sectioned, and double-stained with uranyl acetate-lead citrate. Finally, the slices were observed under a JEM-2100 Plus transmission electron microscope and photographed.

2.10. Quantitative real-time PCR (qPCR)

Total RNA was extracted from leaf and root tissues 15 days after treatment using TRIzol reagent (Invitrogen, Carlsbad, CA). Then, total RNA was reverse transcribed into cDNA using the cDNA Synthesis Kit (Vazyme, Nanjing, China, R223-01). Primers were designed using Primer 5.0 software (Appendix B), and the PCR reaction was performed on a Light Cycler® 96 Real-Time PCR System (Roche, Switzerland). The transcript abundance of genes related to photosynthesis and the AsA–GSH cycle was calculated using the method of $2^{-\Delta\Delta Ct}$ (Gadelha *et al.* 2021; Zhang *et al.* 2022).

2.11. Yield and yield components

Three 1 m^2 sampling plots were selected at maturity (R8) for each treatment. From each sampling plot, 15 soybean plants were randomly selected, and plants per square meter, pods per plant, grains per plant, and 100-grain weight were determined. The yield (t ha^{-1}) was calculated as the average yield per square meter multiplied by 10,000.

2.12. Statistical analysis

Data were analyzed by one-way ANOVA and Duncan's multiple extreme range test at $P<0.05$ using SPSS 25.0 (IBM, Chicago, IL, USA). Graphing was performed using Origin 2024 (OriginLab, Northampton, MA, USA) based on the results of the statistical analysis.

3. Results

3.1. Identification of the optimum Pro-Ca concentration

Foliar application of Pro-Ca significantly attenuated the toxic effect of saline–alkali stress of soybean seedlings (Fig. 1). Compared to CK, Pro-Ca (100 mg L^{-1}) significantly improved dry weight per plant under saline–alkali stress. Similarly, compared to CK, Pro-Ca (100 mg L^{-1}) markedly enhanced P_n of leaves under saline–alkali stress. These results indicated that Pro-Ca (100 mg L^{-1}) can better obtain maximum dry matter accumulation, P_n, and alleviate saline–alkali stress in soybean seedlings.

3.2. Pro-Ca enhances phenotypic parameters under saline–alkali stress

After 15 days of saline–alkali stress, the morphological traits of soybean, i.e., plant height, root length, root dry weight, dry weight per plant, and root/shoot ratio were significantly reduced by 19.6, 24.2, 29.5, 16.8, and 19.9%,

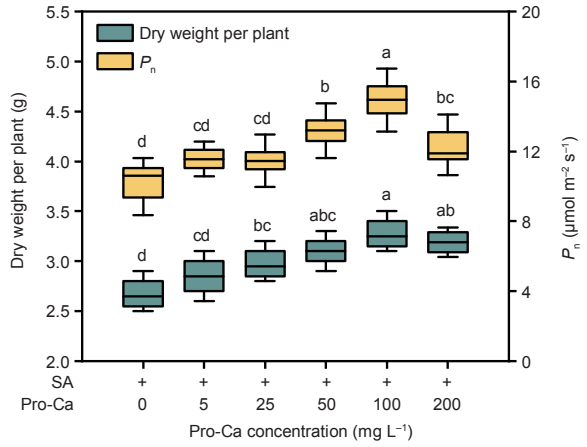

Fig. 1 Effects of different concentrations of prohexadione-calcium (Pro-Ca) on dry weight per plant and net photosynthetic rate (P_n) in soybean.

respectively, compared to CK (Fig. 2-A–F). The digital phenotypic data obtained with the 3D phenotype scanner showed that GI, NDVI, LAI, Hue, and PLA were reduced after 15 d saline–alkali stress treatment and were all significantly lower than CK (Fig. 2-G and H). However, the application of Pro-Ca to saline–alkali treated plants significantly increased plant height, root length, root dry weight, dry weight per plant, root/shoot ratio, NDVI, LAI, Hue, and PLA by 14.7, 19.6, 37.6, 14.1, 29.1, 12.6, 16.2, 3.2, and 16.2%, respectively (Fig. 2-A–H). Moreover, 3D models and phenotypic appearance also visualized that saline–alkali stress inhibited soybean plant growth, but this inhibition was alleviated by exogenous application of Pro-Ca (Fig. 2-I and J; Appendix C). Interestingly, the application of Pro-Ca under non-saline–alkali stress further increased root length, shoot dry weight, root dry weight, and dry weight per plant (Fig. 2-B–E).

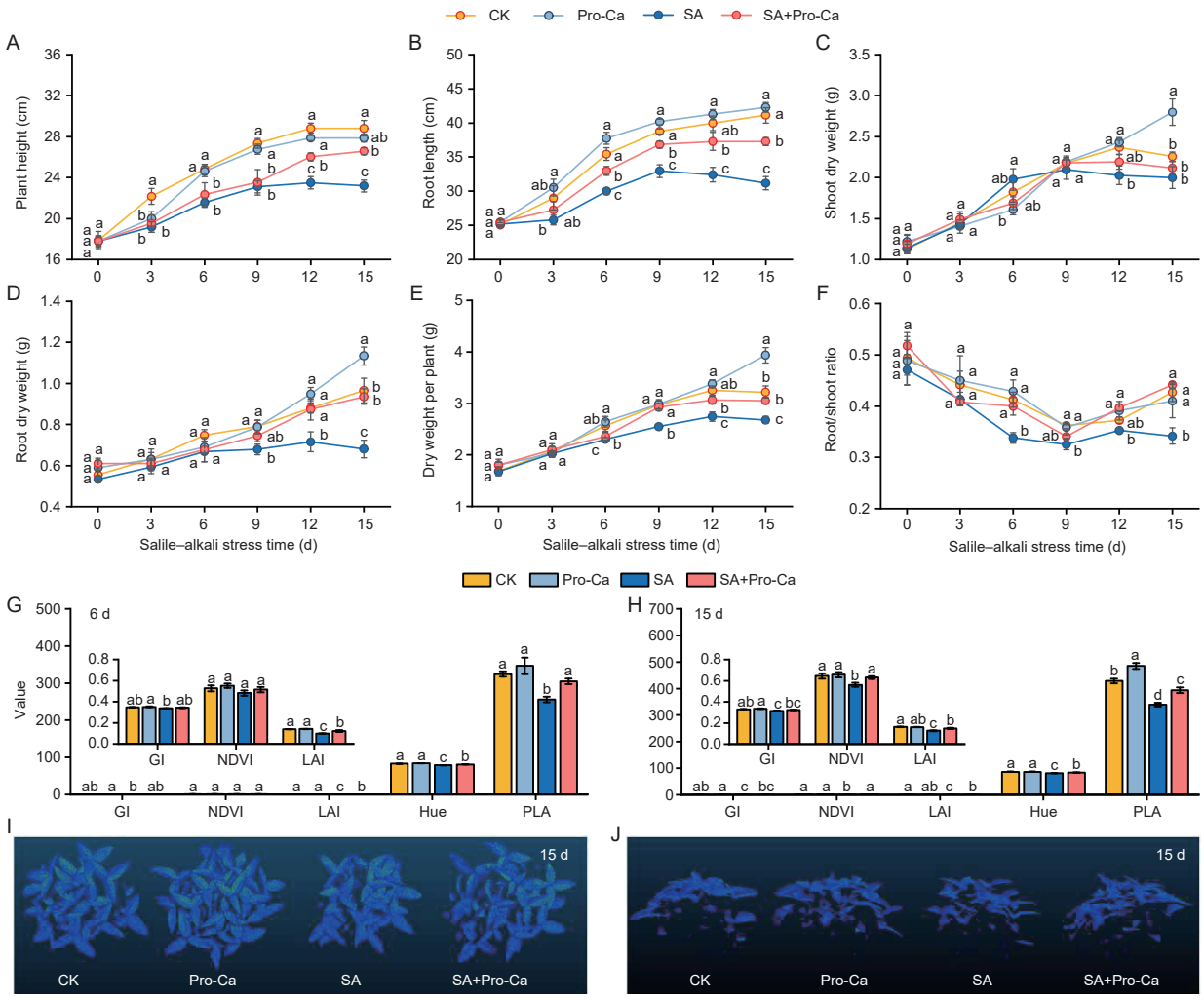

Fig. 2 Amelioration role of prohexadione-calcium (Pro-Ca) on the growth in soybean seedlings under saline–alkali stress. A, plant height. B, root length. C, shoot dry weight. D, root dry weight. E, dry weight per plant. F, root/shoot ratio. G and H, digital phenotypic parameters on days 6 and 15 after treatment, respectively. I, top view of the 3D model of the plant canopy at day 15 after treatment. J, side view of the 3D model of the plant canopy at day 15 after treatment. GI, greenness; NDVI, normalized difference vegetation index; LAI, leaf area index; PLA, projected leaf area. CK, control (normal water); Pro-Ca, foliar Pro-Ca application with 100 mg L^{-1}; SA, 110 mmol L^{-1} saline–alkali stress; SA+Pro-Ca, 110 mmol L^{-1} saline–alkali stress plus foliar Pro-Ca application with 100 mg L^{-1}. Values represent mean±SE (n=3). Different lowercase letters on the error bars indicate significant differences at P<0.05 according to the Duncan's test.

3.3. Pro-Ca triggers the alteration of the transcriptional levels

CK and SA treatments were identified with 1,618 DEGs (412 up-regulated and 1,206 down-regulated), and 938 DEGs (381 up-regulated and 557 down-regulated) were identified in the SA and SA+Pro-Ca groups (Fig. 3-A and D). Exogenous application of Pro-Ca resulted in a significant reduction in the number of down-regulated DEGs in the SA *vs.* SA+Pro-

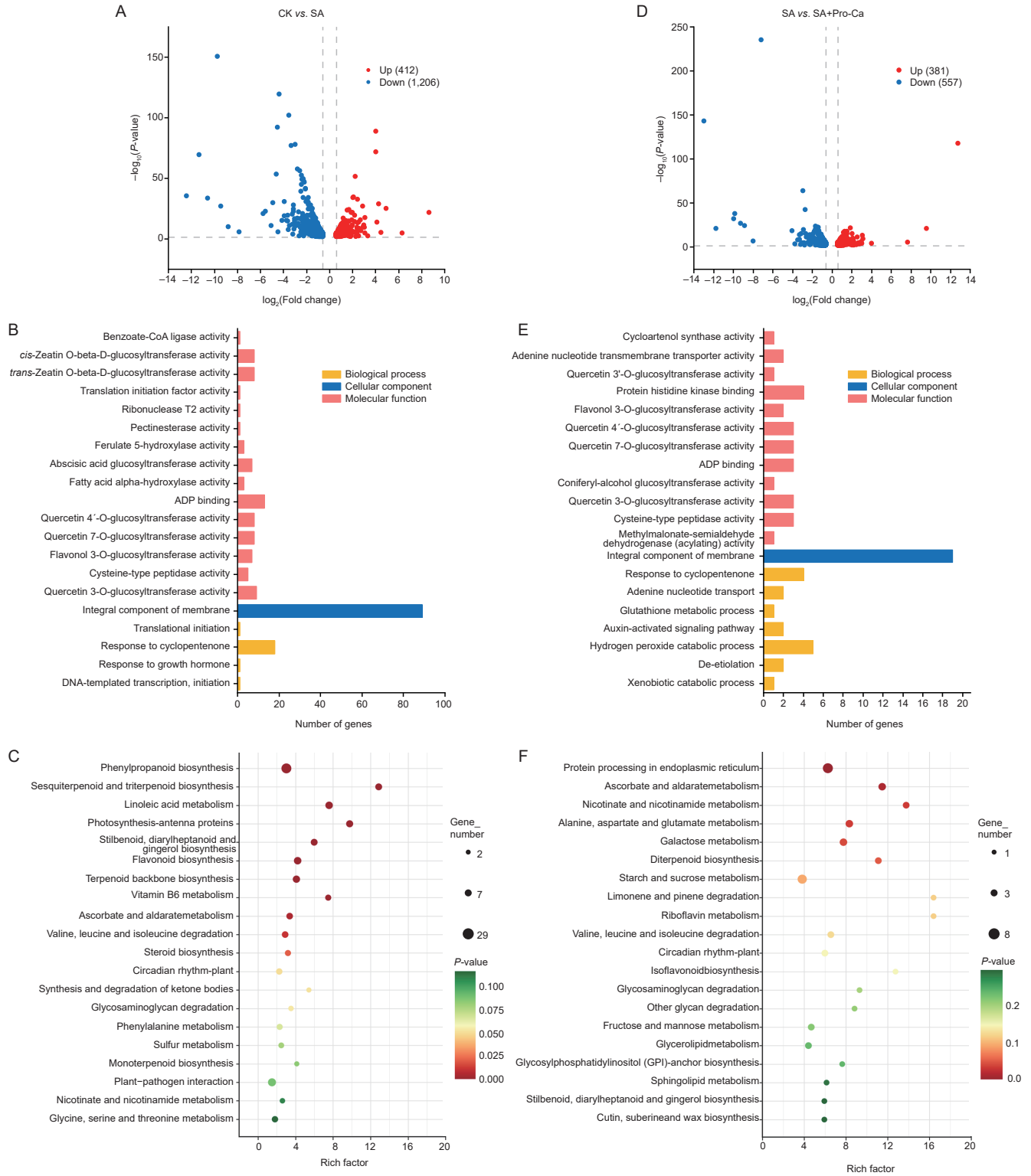

Fig. 3 Prohexadione-calcium (Pro-Ca) triggers the alteration of the transcriptional levels. A–C represent the volcano distribution of differentially expressed genes (DEGs), Gene Ontology (GO) terms of down-regulated DEGs, and Kyoto Encyclopedia of Genes and Genomes (KEGG) enrichment scatter plot of down-regulated DEGs among control (CK) and 110 mmol L^{-1} saline–alkaline stress (SA), respectively. D–F represent the volcano distribution of DEGs, GO terms of up-regulated DEGs, and KEGG enrichment scatter plot of up-regulated DEGs among 110 mmol L^{-1} saline–alkali stress (SA) and 110 mmol L^{-1} saline–alkali stress plus foliar Pro-Ca application with 100 mg L^{-1} (SA+Pro-Ca), respectively.

Ca group compared to the CK *vs*. SA group, suggesting that Pro-Ca has a significant effect on the transcription of genes responding to saline–alkali stress. Further GO enrichment analysis of down-regulated DEGs in the CK *vs*. SA group and up-regulated DEGs in the SA *vs*. SA+Pro-Ca group showed that a large number of DEGs were significantly enriched in the integral component of membrane pathways (Fig. 3-B and E). Furthermore, the KEGG enrichment also revealed that the down-regulated DEGs in the CK *vs*. SA group and the up-regulated DEGs in the SA *vs*. SA+Pro-Ca group were significantly enriched in the ascorbate and aldarate metabolism pathways (Fig. 3-C and F). Therefore, we hypothesized that exogenous application of Pro-Ca might quench saline–alkali stress-induced ROS by activating the AsA–GSH cycle, thereby enhancing the stability of the plant membrane system (e.g., thylakoid, cell, and endoplasmic reticulum membranes), which, in turn, strengthens photosynthetic potential under stress conditions.

3.4. Pro-Ca maintains ionic homeostasis under saline–alkali stress

Saline–alkali stress markedly enlarged the Na^+ content and reduced K^+ content in the leaves, in contrast with the control treatment, resulting in a lower K^+/Na^+ ratio (Fig. 4-A and B). Additionally, the expression levels of *GmSOS1* and *GmNHX1* were notably induced to be up-regulated in saline–alkali-treated plants relative to the saline–alkali treatment (Fig. 4-C and D). Compared to saline–alkali stress, the application of Pro-Ca significantly reduced the Na^+ (32.3%) content in the leaves of stressed seedlings. In contrast, the K^+ content was dramatically higher by 26.4%, contributing to an increase in the K^+/Na^+ ratio to 86.9% (Fig. 4-A and B). Pro-Ca induced higher *GmSOS1* expression without altering *GmNHX1* expression in saline–alkali treated plants, which was from roots rather than leaves, compared with saline–alkali treatment alone (Fig. 4-C and D).

3.5. Pro-Ca elevates photosynthetic capacity under saline–alkali stress

Compared to CK, plants subjected to saline–alkali stress showed significant reductions in Chl_{total}, Chl *a*/*b*, and Car content by 25.7, 43.2, and 14.5%, respectively (Appendix D-a and c). Exogenous Pro-Ca significantly increased the Chl *a*/*b*, Chl_{total}, and Car content by 25.9, 54.4, and 9.8%, respectively, relative to those in saline–alkali stressed plants not treated with Pro-Ca (Appendix D-a and c). In addition, the application of exogenous Pro-Ca alone resulted in a significant increase of 7.3% in Chl_{total} content (Appendix D-a).

Overall, the exogenous application of Pro-Ca had no effect on the gas exchange parameters of soybean leaves under normal growth conditions. However, it increased sucrose and starch content, although the differences were non-significant (Fig. 5-A–F). Compared to CK, saline–alkali stress notably reduced P_n and sucrose content from days 6–15, starch content from days 9–15, C_i/C_a from days 6,12, and 15, and AMC from days 6–15 (Fig. 5-A–F). At day 15, saline–alkali stress reduced P_n, AMC, C_i/C_a, sucrose, and starch content by 51.4, 35.1, 30.1, 28.4, and 32.4%, respectively (Fig. 5-A–F). Differently, L_s at days 6, 12, and 15 were increased, with saline–alkali stress over control (Fig. 5-B). However, saline–alkali-treated plants supplemented with Pro-Ca showed substantially increased P_n at days 6, 9, 12, and 15, AMC at days 12 and 15, C_i/C_a at days 6 and 15, and sucrose and starch contents at days 9, 12, and 15 while drastically decreasing L_s at days 6 and 15 relative to those in CK (Fig. 5-A–F). At day 15, Pro-Ca significantly increased P_n, AMC, C_i/C_a, sucrose, and starch content by 76.4, 67.8, 12.5, 18.1, and 29.7%, respectively, while drastically dwindling L_s by 7.4%, under saline–alkali stress compared to those in the plants not treated with Pro-Ca (Fig. 5-A–F).

3.6. Pro-Ca enhances PSII performance under saline–alkali stress

F_v/F_m, F_v/F_o, ETR, q_P, ΦPSII, and Y(II) were continuously reduced in soybean leaves after saline–alkali stress compared with CK, and exogenous application of Pro-Ca effectively mitigated the adverse impact (Fig. 6-A and B; Appendix E). Additionally, saline–alkali stress also caused a sustained increase in NPQ, but the application of Pro-Ca reduced NPQ relative to the SA group (Fig. 6-A and B). It indicated that the Pro-Ca application to saline–alkali stress-treated plants augmented the photochemical efficiency of

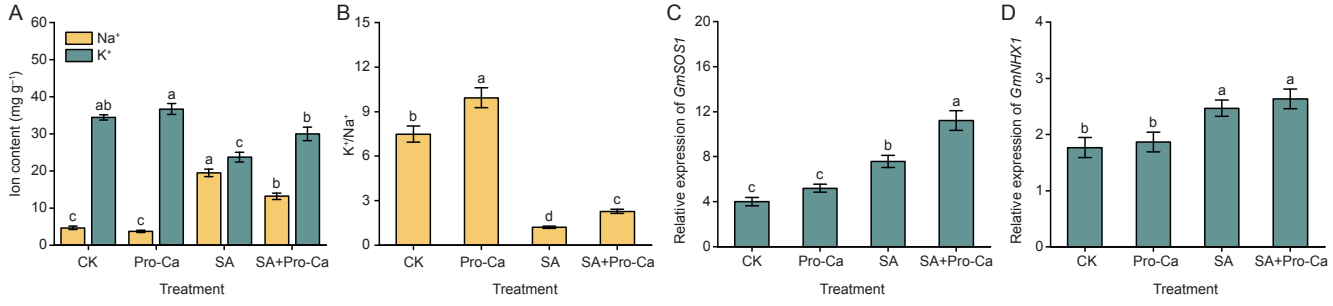

Fig. 4 Effects of prohexadione-calcium (Pro-Ca) on Na^+ and K^+ content (A), K^+/Na^+ ratio (B), and relative expression of *GmSOS1* (C) and *GmNHX1* (D) in soybean leaves under saline–alkali stress. CK, control (normal water); Pro-Ca, foliar Pro-Ca application with 100 mg L^{-1}; SA, 110 mmol L^{-1} saline–alkali stress; SA+Pro-Ca, 110 mmol L^{-1} saline–alkali stress plus foliar Pro-Ca application with 100 mg L^{-1}. Values represent mean±SE (n=3). Different lowercase letters on the error bars indicate significant differences at P<0.05 according to the Duncan's test.

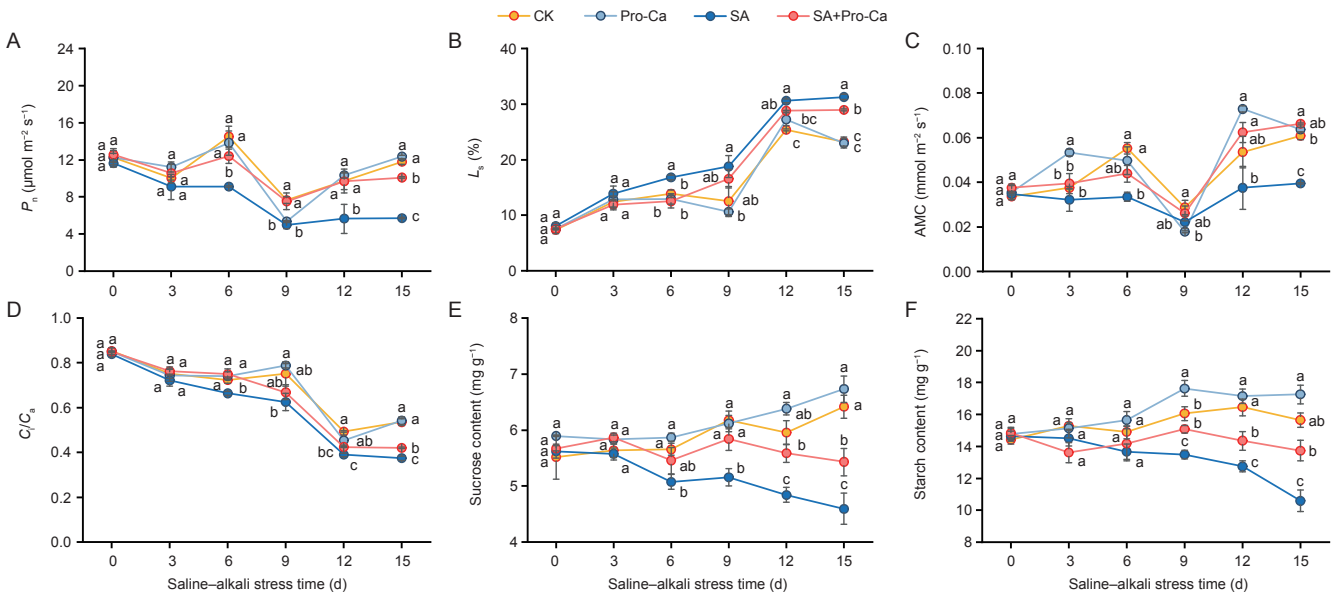

Fig. 5 Effects of prohexadione-calcium (Pro-Ca) on gas exchange parameters and assimilate accumulation in soybean leaves under saline–alkali stress. A, net photosynthetic rate (P_n). B, stomatal limit (L_s). C, apparent mesophyll conductance (AMC). D, C_i/C_a. E, sucrose content. F, starch content. CK, control (normal water); Pro-Ca, foliar Pro-Ca application with 100 mg L^{-1}; SA, 110 mmol L^{-1} saline–alkali stress; SA+Pro-Ca, 110 mmol L^{-1} saline–alkali stress plus foliar Pro-Ca application with 100 mg L^{-1}. Values represent mean±SE (n=3). Different lowercase letters on the error bars indicate significant differences at P<0.05 according to the Duncan's test.

soybean seedlings and reduced the share of excess energy and antenna heat dissipation induced by stress conditions.

The JIP-test analysis of the OJIP curves showed that saline–alkali stress diminished PI_{abs}, S_m, φR_o, φP_o, φE_o, and ψ_o but increased V_I, V_J, M_o, and φD_o relative to CK (Fig. 6-C). However, foliar application of Pro-Ca suppressed the decrease of PI_{abs}, S_m, φR_o, φP_o, φE_o, and ψ_o, while reducing V_I, V_J, M_o, and φD_o, compared to the saline–alkali treatment alone (Fig. 6-C). These results indicated that the application of Pro-Ca to saline–alkali exposed plants reduced the accumulation of Q_A^- in the photosynthetic electron transport chain, improved the electron transport capacity of PSII, restored the assimilation capacity of CO_2, and weakened the feedback inhibition of photosynthetic electron transport.

We performed further analyses of energy distribution and the amount of active reaction centers (RCs) in the electron transport system. The results showed that the application of Pro-Ca under normal growth conditions had no significant effect on the energy distribution and the amount of active RC in the electron transport system of soybean leaves (Fig. 6-C). Under saline–alkali stress, RC/CS and RC/CS_o decreased, and ABS/RC, ABS/CS, DI_o/RC, and DI_o/CS increased, indicating that saline–alkali stress led to a decrease in active RC and an increase in the energy dissipation efficiency of RC (Fig. 6-C). In contrast, Pro-Ca recovered the number of active RC in soybean leaves under saline–alkali stress, as indicated by SA+Pro-Ca increasing RC/CS and RC/CS_o, while reducing ABS/RC, ABS/CS, DI_o/RC, and DI_o/CS, relative to those in saline–alkali stressed plants supplied without Pro-Ca (Fig. 6-C). Furthermore, saline–alkali stress diminished TR_o/RC, TR_o/CS, ET_o/RC, and ET_o/CS, whereas exogenous Pro-Ca mitigated the decreases in the above indicators in soybean leaves under saline–alkali stress, suggesting that more energy could be used to maintain normal operation of PSII electron transport (Fig. 6-C). The membrane model visualizes the specific energy flux changes for each active RC (Fig. 6-D).

3.7. Pro-Ca reactivates the AsA–GSH cycle under saline–alkali stress

Both AsA and GSH contents increased dramatically under saline–alkali stress over the first 3 days, then decreased over the following 12 days, and eventually fell below the control level, a pattern similar but slightly stronger in Pro-Ca-treated plants (Fig. 7-A and D). Saline–alkali stress caused a continuous increase in DHA and GSSG with stress progression, but Pro-Ca treatment of saline–alkali-stressed plants significantly reduced DHA and GSSG content compared to the saline–alkali treatment alone (Fig. 7-B and E). Compared to CK, saline–alkali stress diminished AsA content and considerably increased DHA content in soybean, resulting in a significant lowering of the AsA/DHA ratio, but the application of exogenous Pro-Ca altered this response and increased the AsA/DHA ratio mainly by notably reducing DHA content under saline–alkali stress (Fig. 7-C). Meanwhile, the ratio of GSH/GSSG followed a similar pattern (Fig. 7-F).

APX, GR, DHAR, and MDHAR activities were drastically elevated in the early stage of saline–alkali stress, reaching a maximum on days 9, 6, 3, and 6, respectively, and then gradually weakened and became significantly lower than the control on day 15 (Fig. 7-G–J). This, in turn, increased ROS accumulation and membrane lipid peroxidation as indicated by the increase in H_2O_2 and MDA content with increasing duration of stress treatment until the end of the time course

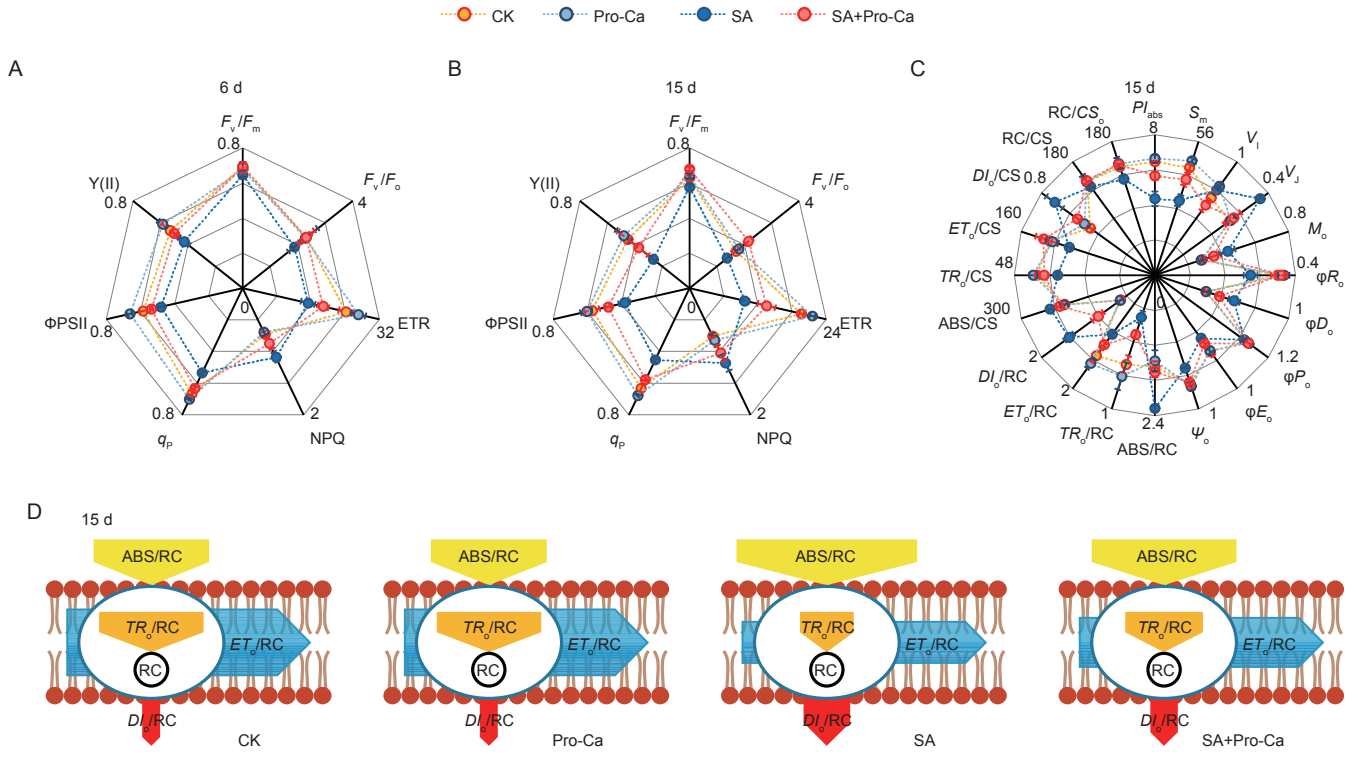

Fig. 6 Effects of prohexadione-calcium (Pro-Ca) on chlorophyll fluorescence parameters in soybean leaves under saline–alkali stress. A and B, distribution of photosystem II (PSII) absorptive energy and excitation energy on days 6 and 15 after treatment. C, quantum yields of linear electron transport chains and energy fluxes per reaction center (RC) and per unit area. D, membrane models of specific energy flux changes per active RC, and the size of the arrows reflects the change in each energy flux. F_v/F_m, maximal photochemical efficiency of PSII; F_v/F_o, potential activity of PSII; ETR, electron transport rate; NPQ, nonphotochemical quenching coefficient; q_P, photochemical quenching coefficient; ΦPSII, effective quantum yield of photochemical energy conversion in PSII; Y(II), PSII actual photochemical quantum yield; PI_{abs}, performance index for energy conservation from photons absorbed by PSII; S_m, storage capacity; V_I, relative variable fluorescence intensity at the I-step; V_J, relative variable fluorescence intensity at the J-step; M_o, approximated initial slope of the fluorescence transient; φR_o, quantum yield for reducing the terminal electron acceptor at the PSI receptor side; φD_o, quantum ratio for heat dissipation; φP_o, maximum quantum yield of initial photochemical efficiency; φE_o, quantum yield for electron transport; Ψ_o, probability of other electron acceptors downstream of QA in the electron transport chain; ABS/RC, absorption flux per RC; TR_o/RC, trapped energy flux per RC; ET_o/RC, electron transport flux per RC; DI_o/RC, dissipated energy flux per RC; ABS/CS, absorption flux per unit cross-sectional area (CS); TR_o/CS, trapped energy flux per CS; ET_o/CS, electron transport flux per CS; DI_o/CS, dissipated energy flux per CS; RC/CS, density of RCs; RC/CS_o, reaction center density.

(Fig. 7-K and L). Interestingly, supplementation of saline–alkali-treated plants with Pro-Ca showed a similar trend but considerably increased APX, GR, and DHAR activities (Fig. 7-G–J), which resulted in lower H_2O_2 and MDA contents (Fig. 7-K and L) compared to saline–alkali stress alone.

3.8. Pro-Ca protects leaf ultrastructure against saline–alkali damage

The changes in the ultrastructure of Pro-Ca soybean mesophyll cells with or without exogenous application of Pro-Ca under no and saline–alkali stress are shown in (Fig. 8). Chloroplasts of soybean leaves supplemented with or without Pro-Ca under no saline–alkali conditions exhibited a typical ellipsoid shape and adhered tightly to the inner side of the cell wall, with sequential stacking of thylakoids into stacks to form compact grana lamellae, more starch granules and mitochondria with intact mitochondrial inner membranes, and fewer osmiophilic granules (Fig. 8-A–D). Exposure of plants to saline–alkali stress severely damaged the ultrastructure, as evidenced by swollen chloroplasts, reduced size of starch granules, swollen, structurally blurred and partially ruptured grana lamellae, and fewer mitochondria but markedly more osmiophilic granules (Fig. 8-E and F). However, for Pro-Ca-treated seedlings under saline–alkali stress conditions, chloroplast morphology was intact, basal lamellae were loosened but still structurally clear, starch granules were full, osmiophilic granules were remarkably reduced, and mitochondria were structurally intact and with well-defined inner membranes (Fig. 8-G and H). These results indicated that the application of exogenous Pro-Ca considerably alleviated saline–alkali stress-induced cellular damage and effectively protected the inner membrane structure of chloroplasts, which may provide a powerful foundation for photosynthetic activities in plants.

3.9. Pro-Ca up-regulates the transcript levels in photosystem and AsA–GSH cycle pathway genes under saline–alkali stress

The expression of genes related to photosynthesis and the AsA–GSH cycle in soybean was assessed at the

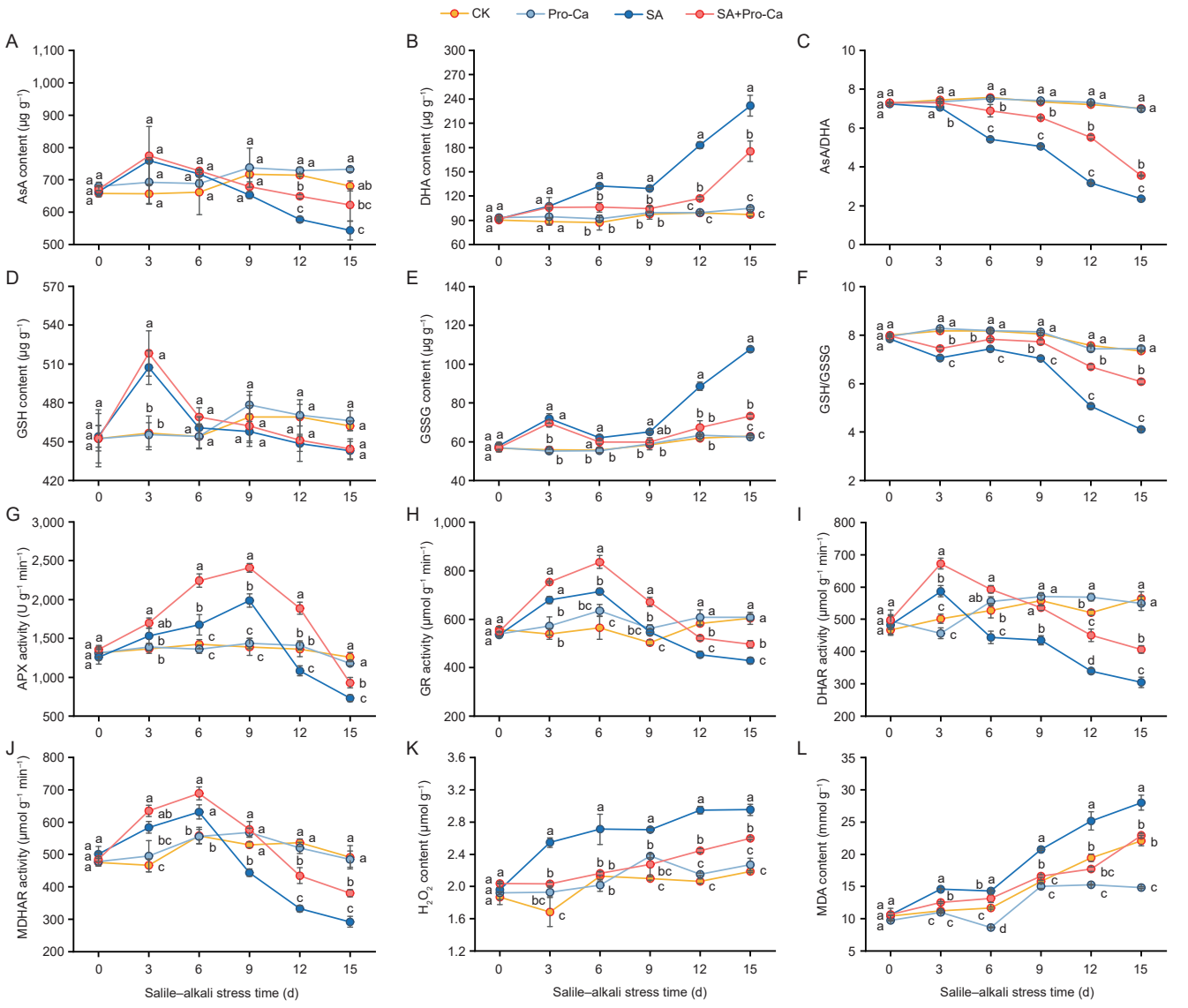

Fig. 7 Effects of prohexadione-calcium (Pro-Ca) on ascorbate (AsA)–glutathione (GSH) cycle in soybean leaves under saline–alkali stress. A, AsA. B, dehydroascorbate (DHA). C, AsA/DHA. D, GSH. E, oxidized glutathione (GSSG). F, GSH/GSSG. G, ascorbate peroxidase (APX). H, glutathione reductase (GR). I, dehydroascorbate reductase (DHAR). J, monodehydroascorbate reductase (MDHAR). K, hydrogen peroxide (H_2O_2). L, malondialdehyde (MDA). CK, control (normal water); Pro-Ca, foliar Pro-Ca application with 100 mg L^{-1}; SA, 110 mmol L^{-1} saline–alkali stress; SA+Pro-Ca, 110 mmol L^{-1} saline–alkali stress plus foliar Pro-Ca application with 100 mg L^{-1}. Values represent mean±SE (n=3). Different lowercase letters on the error bars indicate significant differences at P<0.05 according to the Duncan's test.

transcriptional level (Fig. 9). On day 15 after saline–alkali stress, the expression levels of the *Lhca*, *PsaA*, and *PsaB* genes in PSI, the *PsbA*, *PsbC*, and *Cytb6f* genes in PSII, and *APX*, *GR*, *DHAR*, and *MDHAR* genes, critical enzymes of the AsA–GSH cycle, were significantly down-regulated relative to the control. However, the expression levels of *Lhca*, *PsaB*, *PsbA*, *Cytb6f*, *APX*, *GR*, and *DHAR* were notably up-regulated by Pro-Ca in saline–alkali-treated plants compared to saline–alkali treatment alone. Additionally, there was no significant difference in the expression levels of *PsaA*, *PsbC*, and *MDHAR* in the SA+Pro-Ca treatment compared to SA. It was worth noting that the application of Pro-Ca under non-stress conditions likewise remarkably increased the transcript levels of *Cytb6f*.

3.10. Pro-Ca improves yield under saline–alkali stress

Saline–alkali treatments significantly reduced grains per plant, 100-grain weight, and yield by 9.8, 11.7, and 20.4%, respectively, compared to CK, while the effect on pods per plant was not significant (Fig. 10-A–D). In contrast, the SA+Pro-Ca treatment resulted in 13.0% (P<0.05) increase in soybean yield, 9.4% (P>0.05) increase in pods per plant, 5.8% (P>0.05) increase in grains per plant, and 6.7% (P>0.05) increase 100-grain weight compared to the SA treatment (Fig. 10-A–D).

4. Discussion

4.1. Pro-Ca reduces Na^+ uptake to alleviate saline–alkali stress in soybean

Saline–alkali-induced growth performance inhibition was

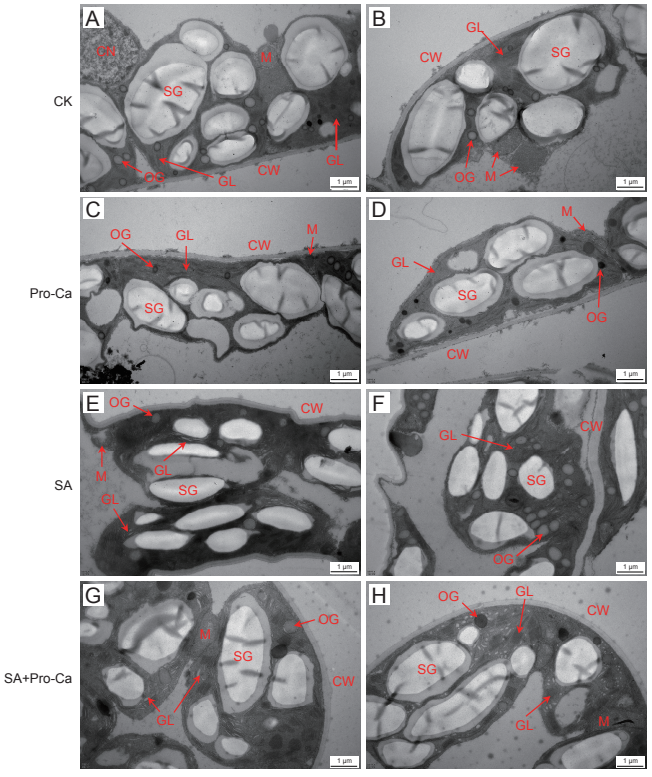

Fig. 8 Effects of prohexadione-calcium (Pro-Ca) on the ultrastructure in soybean leaves under saline–alkali stress. GL, grana lamella; SG, starch granules; M, mitochondria; OG, osmiophilic granules; CN, cell nucleus; CW, cell wall. CK, control (normal water); Pro-Ca, foliar Pro-Ca application with 100 mg L^{-1}; SA, 110 mmol L^{-1} saline–alkali stress; SA+Pro-Ca, 110 mmol L^{-1} saline–alkali stress plus foliar Pro-Ca application with 100 mg L^{-1}.

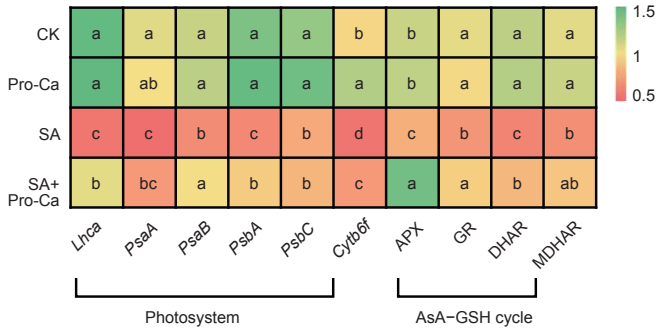

Fig. 9 Effects of prohexadione-calcium (Pro-Ca) on the transcript levels in photosystem-related genes and ascorbate (AsA)–glutathione (GSH) cycle enzyme-related genes under saline–alkali stress. CK, control (normal water); Pro-Ca, foliar Pro-Ca application with 100 mg L^{-1}; SA, 110 mmol L^{-1} saline–alkali stress; SA+Pro-Ca, 110 mmol L^{-1} saline–alkali stress plus foliar Pro-Ca application with 100 mg L^{-1}. Different lowercase letters indicate significant differences at $P<0.05$ according to the Duncan's test.

reflected in reduced plant height, root length, shoot dry weight, root dry weight, and root/shoot ratio (Fig. 2-A–F), which is consistent with the findings of Zhang *et al.* (2021) in cotton and Rasool *et al.* (2013) in chickpea. This inhibition is likely due to the complex interaction of ionic toxicity, oxidative stress, photosynthetic damage, and structural disruption (Fan *et al.* 2021; Peña-Calzada *et al.* 2023). Under saline–alkali stress, Na^+ is transported from roots to leaves with transpiration flow and eventually accumulates continuously in the leaves (Liu *et al.* 2019; Zhang *et al.* 2022). Further, excessive Na^+ enrichment causes plasma membrane depolarization, leading to the opening of K^+ outward rectifier channels, which in turn results in excessive K^+ efflux and reduced the K^+/Na^+ ratio (Gupta *et al.* 2017). In the course of natural evolution, plants have derived a multitude of active defense strategies from avoiding Na^+ accumulation: (i) Na^+ exclusion back into the apoplast; (ii) Na^+ compartmentalization into the vacuole; (iii) phloem re-circulation of Na^+; (iv) preferential allocation of Na^+ to older leaves over newer leaves and direct Na^+ excretion to the leaf surface (halophytes only), etc. (Gadelha *et al.* 2021). In the present study, the transcript levels of the two regulated Na^+ transporter genes, *GmSOS1* and *GmNHX1*, were significantly up-regulated under saline–alkali stress compared to non-stressed plants (Fig. 4-C and D). This suggests that the Na/H anti-transporter SOS1 located in the plasma membrane, is able to induce the exclusion of Na^+ from the root system by utilizing the proton gradient generated by the H-ATPase, while the NHX transporter protein located in the vacuole membrane facilitates the Na^+ entry into the vacuoles

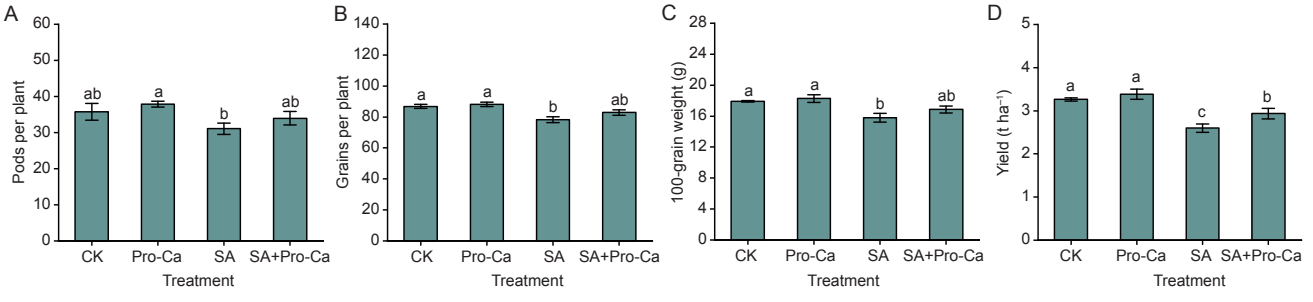

Fig. 10 Effects of prohexadione-calcium (Pro-Ca) on yield and yield components of soybean under saline–alkali stress. A, pods per plant. B, grains per plant. C, 100-grain weight. D, yield. CK, control (normal water); Pro-Ca, foliar Pro-Ca application with 100 mg L^{-1}; SA, 110 mmol L^{-1} saline–alkali stress; SA+Pro-Ca, 110 mmol L^{-1} saline–alkali stress plus foliar Pro-Ca application with 100 mg L^{-1}. Values represent mean±SE (n=3). Different lowercase letters on the error bars indicate significant differences at $P<0.05$ according to the Duncan's test.

(Cheng *et al.* 2019; Sun *et al.* 2019; Zhang *et al.* 2022). These mechanisms likely play an important role in soybean adaptation to salinity stress, helping to maintain cellular ion homeostasis and promoting plant growth. Similar findings were observed in rice, where activation of the *OsSOS1* gene led to a reduced Na^+ in-flow in the root elongation zone, thus limiting its transport to the leaves (Liu *et al.* 2019). However, we further observed significant accumulation of Na^+ in the leaves (Fig. 4-A), indicated that these defense strategies have exceeded the threshold and are insufficient to cope with prolonged stress. On the other hand, the plant's capacity to withstand stress still needs to be urgently further evaluated.

The current study showed that the exogenous plant growth regulator Pro-Ca has been used to promote the growth in soybean (Feng *et al.* 2021), rice (Liu *et al.* 2024), *Vicia faba* (Bekheta *et al.* 2009), and *Brassica napus* L. (Deng P *et al.* 2024) under salinity or/and combined alkali stress. Exogenous Pro-Ca treatment of plants subjected to saline–alkali stress effectively mitigated the toxic effects induced by saline–alkali stress, as evidenced by the increase in plant height, root length, shoot dry weight, root dry weight, root/shoot ratio, and K^+/Na^+ ratio (Figs. 2-A-F and 4-B). The most significant effects were observed at 100 mg L^{-1} Pro-Ca, which resulted in the improved P_n and dry weight per plant, consistent with the 3D modeled phenotypes (Figs. 1 and 2-I and J). One possible explanation for the improved root dry weight, which may be associated with enhanced root elongation and lateral root development, is that Pro-Ca triggers hormone changes (e.g., auxin and cytokinins) in root cells (Deng R *et al.* 2024), which help enhance tolerance to saline–alkali stress. Although hormone metabolism was not the focus of our study, it represents a critical pathway for future in-depth exploration of its mechanisms. Additionally, the increase in plant height and shoot dry weight was associated with an increase in biomass partitioning from aboveground to roots, which may be explained by improved cell wall enlargement and tissue extensibility, photosynthesis, and assimilate synthesis (Ahmad *et al.* 2018). Furthermore, Pro-Ca application in soybean seedlings under saline–alkali stress further up-regulated the expression of *GmSOS1*, whereas it did not notably affect the expression of *GmHNX1* compared to the saline–alkali treatment alone (Fig. 4-C and D). In other words, Pro-Ca treatment inhibited Na^+ entry into cellular nonselective cation channels, thereby effectively preventing Na^+ influx, which in turn induced greater retention of K^+ within the cell and consequently increased the K^+/Na^+ (Fig. 4-A and B). Overall, Pro-Ca served to maintain ion homeostasis, reduce nutrient imbalance, and stimulate growth under saline–alkali stress conditions (Bekheta *et al.* 2009; Becker *et al.* 2020; Feng *et al.* 2021; Deng R *et al.* 2024; Liu *et al.* 2024).

The results of the current study showed that saline–alkali stress remarkably reduced both GI and Hue (Fig. 2-G and H), revealed that saline–alkali stress diminished the photosynthetically active radiation of the plant manifested as a reduction in leaf absorption of red, blue, and green light, as well as a reduction in the reflectance of near-infrared light (Tripodi *et al.* 2024), which is supported by the reduction in the content of Chl *a* (absorption of red light) and Chl *b* (absorption of blue-violet light) content in soybean leaves under saline–alkali stress (Appendix D-a), which is consistent with the findings of Zhao *et al.* (2023). Moreover, the uptake of photosynthetically active radiation was also closely related to canopy area and aboveground biomass, and the reduction in LAI, PLA, and NDVI induced by saline–alkali stress (Fig. 2-G and H) indicated that the decreased uptake of photosynthetically active radiation led to lower assimilate synthesis and the negative feedback inhibited aboveground growth and canopy development (Fig. 2-I and J) (Zhao *et al.* 2023; Tripodi *et al.* 2024). However, Pro-Ca treatment effectively mediated the effects of saline–alkali stress on soybean spectral indices, increasing GI, Hue, LAI, PAL, and NDVI (Fig. 2-G and H). These results further demonstrated the positive regulatory effect of Pro-Ca on the soybean canopy, promoting light energy interception by increasing the chlorophyll content and maintaining the canopy area, thereby increasing the accumulation of aboveground biomass (Großkinsky *et al.* 2015). The 3D images also visually confirmed the mitigating effect of Pro-Ca on the development of soybean canopies under saline–alkali stress (Fig. 2-I and J). NDVI is recognized as a key indicator of plant developmental health and nutrient status. This corroborates the results of Pro-Ca, which reduce Na^+ influx, as reduced Na^+ accumulation contributed to increased uptake of nutrients such as K^+, Ca^{2+}, and Mg^{2+} (Alam *et al.* 2019), thus improving the plant's nutritional status.

4.2. Pro-Ca enhances photosystem performance to promote assimilate accumulation

Previous studies revealed that photosynthesis contributes about 95% of biomass and that stomatal and non-stomatal limitations are the main factors responsible for plants' reduced photosynthetic carbon assimilation capacity (Feng *et al.* 2021). In this study, saline–alkali stress reduced P_n, C_i/C_a, and AMC, while L_s increased in soybean leaves compared to CK (Fig. 5-A–D), indicating that stomatal limitation resulted in an insufficient supply of substrates for photosynthetic carbon fixation, causing a decrease in P_n. In addition, AMC might be used to assess Rubisco activity (Xu *et al.* 2019; Salesse-Smith *et al.* 2025). The decrease in AMC and photosynthetic pigment content under saline–alkali stress showed reduced carbon fixation in the Calvin cycle, resulting in non-stomatal limitation, which strongly supports the reduction in starch and sucrose contents in stressed plants concomitant with a reduction in starch granule size (Fig. 5-E and F). In contrast, a surprising observation in our study was that supplementation with Pro-Ca effectively reversed the adverse impacts of saline–alkali stress on photosynthetic potential. Pro-Ca treatment led to a significant increase in P_n, AMC, C_i/C_a, Chl_{total}, and Car, and a reduction in L_s in the SA+Pro-Ca treatment compared to SA (Fig. 5-A–D; Appendix D-a and c). This emphasizes the positive role of exogenous Pro-Ca in ameliorating stomatal limitation and non-stomatal limitations for P_n enhancement under saline–alkali stress, which might be attributed to increased light energy capture (ATP sufficiency), increased CO_2 diffusion into the mesophyll cells (carbon substrate sufficiency), and elevated Rubisco

activity (accelerated carbon fixation) (Feng *et al.* 2021). Furthermore, the increase in the carbon content assimilates sucrose and starch, and the improvement in leaf ultrastructure also proved this inference in reverse (Figs. 5-E, F and 8-G, H). Our results are consistent with studies in various crops (e.g., rice, oilseed rape, strawberry, and fava bean) (Bekheta *et al.* 2009; Becker *et al.* 2020; Deng P *et al.* 2024; Deng R *et al.* 2024). Supplementation with plant growth regulators has been reported to increase chlorophyll content and thereby P_n in salt-stressed plants, which might be attributed to enhanced uptake of Mg^{2+} as a chelating central metal element centrally located in the chlorophyll porphyrin ring (Alam *et al.* 2019; Zhao *et al.* 2024). Furthermore, carotenoids, which is located in the photoreaction center, also acts to protect the membrane lipid phase by modulating photoprotection (quenching the excited trilinear states of Chl *a* and Chl *b*) and antioxidant (bursting the singlet oxygen) and the addition of Pro-Ca may have increased the phytoene synthase (PSY) activity, thereby promoting the Car biosynthesis (Parida and Jha 2013; Sharma *et al.* 2016).

The intrinsic influence of environmental factors on PSII and PSI can be reflected by chlorophyll fluorescence parameters (Tang *et al.* 2021; Wang *et al.* 2021). The current study observed that F_v/F_m, F_v/F_o, and ETR were significantly reduced under saline–alkali stress (Fig. 6-A and B). This finding is consistent with previous studies in *Brassica juncea* (Wani *et al.* 2017) and *Lycium barbarum* (Zhang *et al.* 2019), which indicate that saline–alkali induces the onset of photoinhibition, the blockage of electron transport from primary to secondary receptors, and the inhibition of the Q_A reduction process caused by the reduction in the number of active RCs. Under saline–alkali stress, ΦPSII, q_P, and Y(II) also reduced remarkably, while NPQ increased (Fig. 6-A and B). Increasing NPQ assisted the photosystem in dissipating excess excitation energy to adapt to photosynthesis-decrease-induced photodamage, which may be attributed to the contradiction between the lower energy capture efficiency of the PSII reaction centers and the loss of q_P and excess reducing capacity, coupled with the blocked electron transport that drives significant energy dissipation to reduce the actual photosynthetic rate of PSII (Miranda *et al.* 2016; Bae *et al.* 2024). This is consistent with observations of grana lamellae rupture and mitochondria reduction under saline–alkali stress (Fig. 8-E and F). Noteworthy, Pro-Ca was applied to plants exposed to saline–alkali, the negative effects of saline–alkali on multiple fluorescence parameters were effectively counteracted, as manifested by increases in F_v/F_m, F_v/F_o, ETR, q_P, ΦPSII, and Y(II) (Fig. 6-A and B). Our results were supported by Feng *et al.* (2021), that Pro-Ca effectively reduced photoinhibition and increased electron transport efficiency of PSII in saline–alkali stressed soybean. Additionally, a decrease in NPQ was observed by supplementation of Pro-Ca into saline–alkali stress-treated soybean plants. These results suggest that Pro-Ca enhances biochemical homeostasis in the photosynthetic response by promoting Q_A reduction to reduce heat dissipation by enhancing energy capture and electron transport activity of PSII, which helps to maintain the integrity of the membrane structure of the thylakoid and reduces the loss of dry matter (Alam *et al.* 2019; Gadelha *et al.* 2021; Luo *et al.* 2021). Promisingly, the application of Pro-Ca to soybean seedlings exposed to saline–alkali resulted in stable chloroplast morphology, with loosened yet structurally intact grana lamellae. Mitochondria were also structurally intact, with well-defined internal cristae, full starch granules, and fewer osmiophilic granules (Fig. 8-G and H). Meanwhile, integral membrane components, which were downregulated under saline–alkali stress, were dramatically upregulated with Pro-Ca supplementation (Fig. 3-B and E). These results support the beneficial role of exogenous Pro-Ca in regulating cellular structure and highlight a basis for metabolic activities that depend on its structure-shaping function.

To advance the interpretation of how Pro-Ca responds to PSII photoinhibition induced by saline–alkali stress, we performed a JIP-test analysis of the chlorophyll fluorescence kinetics (OJIP curve). Parameters such as M_o, S_m, φE_o, φP_o, and ψ_o mainly reflect changes on the PSII receptor side (Tang *et al.* 2021). PSII receptor side mainly includes components like the primary quinone receptor (Q_A), secondary quinone receptor (Q_B), and plastoquinone (PQ), etc. (Zhang *et al.* 2019). Our results indicate that saline–alkali stress led to a smaller electron acceptor storage capacity (S_m) on the PSII receptor side of the leaf. This reduction resulted in a decreased probability of electron transport to the electron acceptors in the ETC beyond Q_A^- (φE_o), with more light energy being used to reduce Q_A, accelerating the reduction of QA (M_o) (Fig. 6-C) (Tang *et al.* 2021). Similarly, V_I and V_J represent the number of RCs closed at points I and J, respectively, i.e., the accumulation of Q_A^- (Tang *et al.* 2021; Wang *et al.* 2021). Saline–alkali stress increased V_I and V_J (Fig. 6-C), indicating that the large accumulation of Q_A^- in the photosynthetic electron transport chain increased the feedback inhibition of photosynthetic electron transport, resulting in the weakening of electron transport capacity. Consistent results were also obtained in the study of *L. barbarum* L. by Zhang *et al.* (2019). Conversely, the application of Pro-Ca increased V_I, V_J, S_m, φE_o, φP_o, and ψ_o while decreasing M_o (Fig. 6-C) in the photochemical reactions of plants under saline–alkali stress. These results strongly support the argument that Pro-Ca increases the number of RCs by reducing the accumulation of Q_A^- in the electrically transported chain and thereby enhances the electron transport efficiency of PSII (Bae *et al.* 2024). Additionally, φD_o indicates the proportion of excess light energy dissipated by plant heat (Zhang *et al.* 2019). The reduction of φD_o induced by Pro-Ca treatment under saline–alkali stress revealed lower photosystem energy dissipation, meaning more light energy was utilized for electron transport, consistent with the changes in NPQ (Fig. 6-A and B). Moreover, Pro-Ca-mediated increase in φR_o contributed to protecting PSI receptor side terminal electron acceptors and ferredoxin-$NADP^+$ reductase (FNR) activity (Sun *et al.* 2016; Zhu *et al.* 2018). Additionally, specific activity, which is the active per unit cross-sectional area (CS) or unit RC of illuminated material when PQ is in the reduced state, provides a more accurately reflecting of the status of light energy absorption, translation, and dissipation in plant photosynthetic organs. Saline–alkali stress decreased RC/CS, RC/CS_o, TR_o/RC, TR_o/CS, ET_o/RC, and ET_o/CS, together with an increase in ABS/RC, ABS/CS, DI_o/RC, and DI_o/CS, whereas application of Pro-Ca to plants subjected to saline–alkali stress reversed the trend of these parameters, suggesting that the

reduction in the active RCs due to saline–alkali stress as well as the lower light conversion efficiency can be alleviated by Pro-Ca and more light energy is used for RC activity, which contributes to the lower energy dissipation efficiency of RCs (Fig. 6-C) (Zhang *et al.* 2019). Convincingly, the qPCR results confer additional evidence for our extrapolation. We observed that transcript expression of *Lhca* (encoding photosynthesis-antenna proteins), *PsaA* and *PsaB* (encoding PSI), *PsbA* and *PsbC* (encoding PSII), and *Cytb6f* (an intermediate electron transporter linking PSII to PSI) was notably down-regulated under saline–alkali stress, whereas it was remarkably up-regulated in response to the addition of Pro-Ca (except for *PsaA* and *PsbC* which had no significant difference) compared to saline–alkali treatment alone (Fig. 9). Yi *et al.* (2007) pointed out that the loss of PSII reaction center proteins (encoded by *PsbA*) and inner light-harvesting complex proteins (encoded by *PsbC*) could be attributed to the absence of *PsbP* proteins. Up-regulation of the expression of the above photosystem-responsive genes was also found to enhance the adaptation of PSI and PSII to saline–alkali stress in soybean (Yang *et al.* 2018; Zhao *et al.* 2023; Bae *et al.* 2024), alfalfa (Wang *et al.* 2021), and *Robinia pseudoacacia* (Lu *et al.* 2023). Overall, the application of Pro-Ca is one of the primary mechanisms to enhance the photosynthetic performance (PI_{abs}) of soybean under saline–alkali stress *via* increasing the number of PSII active RCs and electron transport while reducing energy dissipation.

4.3. Pro-Ca reactivates the AsA–GSH cycle to efficiently scavenge ROS

The current study demonstrated that H_2O_2 and MDA contents increased with stress duration, while the levels of two non-antioxidants (AsA and GSH) as well as four antioxidants (APX, GR, DHAR, and MDHAR) initially increased and then decreased with the stress progression (Fig. 7). In the early stage, lower levels of H_2O_2 were efficiently scavenged by the turnover of antioxidants and non-antioxidants (Zhu *et al.* 2024). However, as stress continued, the accumulation of H_2O_2 exceeded the scavenging capacity of the AsA–GSH cycle, resulting in oxidative damage to the cells (Mittler 2017; Wang *et al.* 2024). However, numerous studies have shown that the addition of exogenous plant growth regulators, such as melatonin (Zhao *et al.* 2023), brassinolide (Alam *et al.* 2019), γ-aminobutyric acid (Zhao *et al.* 2024), and abscisic acid (Hu *et al.* 2021), could enhance the activity of the AsA–GSH cycle in plants and effectively mitigate the oxidative stress caused by ROS. Interestingly, through KEGG enrichment analysis, we localized a critical pathway whereby ascorbate and aldarate metabolism were significantly down-regulated under saline–alkali stress, and this down-regulation trend was dramatically reversed by Pro-Ca application (Fig. 3-C and F). Therefore, we hypothesized that the exogenous application of Pro-Ca might quench ROS by activating the AsA–GSH cycle in response to soybean saline–alkali stress. Similarly, in the present study, the Pro-Ca-mediated enhancement of APX activity and decrease in H_2O_2 content under saline–alkali stress indicated that the AsA–GSH cycle was reactivated in response to oxidative stress (Fig. 7-G and K). This is because APX detoxification of H_2O_2 is the first step in the AsA–GSH cycle. Davletova *et al.* (2005) demonstrated that the chloroplast H_2O_2 scavenging system would be disrupted by cytoplasm APX deficiency-induced disintegration. Application of Pro-Ca to saline–alkali stressed soybean plants enhanced GR activity, contributing to the NADPH-dependent reduction of GSSG to GSH, thereby maintaining the GSH/GSSG ratio by increasing GSH content and reducing GSSG content (Fig. 7-D–F and H). The GSH/GSSG is an abundant redox buffer in plant cells and is involved in ROS scavenging and signal transduction (Hasanuzzaman *et al.* 2020). Moreover, successive GSSG reductions by GR, in turn, supplied GSH to DHAR along with the maintenance of the $NADP^+$ pool to sustain photosynthetic electron transport, which contributed to the reduction of heat dissipation and photoinhibition (Raja *et al.* 2017). We observed enhanced DHAR and MDHAR activities in salt-treated soybean plants sprayed with Pro-Ca compared to saline–alkali stress (Fig. 7-I and J). This indicates that monodehydroascorbate (MDHA) produced from the reduction of H_2O_2 by APX using AsA as a substrate is either efficiently reduced to AsA by MDHAR or converted to DHA *via* a spontaneous imbalance process and then regenerated by DHAR using GSH as an electron donor. This process allows AsA to re-enter the cycle, equilibrating the high AsA/DHA couple (Fig. 7-C) and the generation of GSSG (Alam *et al.* 2019). Pro-Ca mediates has also been shown to mediate salt tolerance in oilseed rape by increasing AsA level and APX activity, as reported in the study by Deng P *et al.* (2024). In addition, Pro-Ca treatment reversed the saline-induced reduction in *APX*, *GR*, *DHAR*, and *MDHAR* transcript levels, further confirming that Pro-Ca plays a positive regulatory role in reactivating the AsA–GSH cycle (Fig. 9). Overall, Pro-Ca-mediated reactivation of the AsA–GSH cycle contributes to scavenging of excessive ROS and helps to maintain lower levels of MDA in mesophyll cells (Fig. 7-K and L), which plays a fundamental role in enhancing saline–alkali tolerance in soybean.

4.4. Pro-Ca improves soybean yield under saline–alkali stress

Saline–alkali stress reduces soybean yield by decreasing grains per plant and 100-grain weight (Fig. 10). Similar results have been reported by Akram *et al.* (2017) in soybean studies. Pro-Ca significantly increased soybean yield by 13.0% under saline–alkali stress compared to saline–alkali treatment alone (Fig. 10), which could be attributed to the common trade-off between pods per plant, grains per plant, and 100-grain weight. Overall, Pro-Ca increased soybean productivity under saline–alkali stress by improving photosynthetic capacity and reducing toxic Na^+ accumulation in pods per plant, grains per plant, and 100-grain weight; its in-depth molecular mechanism still needs further study.

4.5. Long-term effects of Pro-Ca on plants and the environment and use strategies

Pro-Ca, as a plant growth regulator, can significantly regulate plant growth in the short term, but its long-term effects still need carefully evaluation. Long-term application of Pro-Ca might lead to adaptive changes in the plant's response

to inhibition of gibberellin synthesis, affecting its natural growth rhythms (Rademacher 2015). Meanwhile, Pro-Ca might affect gene expression in plants through epigenetic mechanisms (e.g., DNA methylation), which in turn might have long-term effects on future generations of plants (Jiang *et al*. 2023). Additionally, the long-term environmental impacts of the use of plant growth regulators have been confirmed by several studies. Long-term use of Pro-Ca may remain in the soil, affecting soil microbial community structure and function (Bukhat *et al.* 2020); it may enter water bodies through surface runoff and have toxic effects on aquatic organisms (e.g., algae, fish) (Wang *et al.* 2020); it may also be passed through the food chain, affecting the survival and reproduction of non-target organisms (e.g., insects, birds) (Desneux *et al.* 2007). Therefore, strictly controlling the dose and frequency of exogenous plant growth regulators is an essential strategy to achieve a win–win situation for both the environment and the plant, while incorporating agricultural management practices (e.g., crop rotation and intercropping) to minimize dependence on a single plant growth regulator.

In summary, our results demonstrated at the phenotypic, physiological, and transcriptional levels that Pro-Ca increases soybean yield under saline–alkali stress by modulating ion homeostasis, ascorbate–glutathione defense, and photosynthesis (Fig. 11). However, there are still some limitations: (i) the molecular mechanisms have not been elucidated completely; (ii) optimization of different application times and doses; (iii) the effects and potential risks of long-term applications; and (iv) the studies have mostly focused on laboratory or short-term field experiments, and there is a lack of data from long-term field experiments. Therefore, future studies should focus on addressing these issues to ensure the safe, effective, and sustainable application of Pro-Ca.

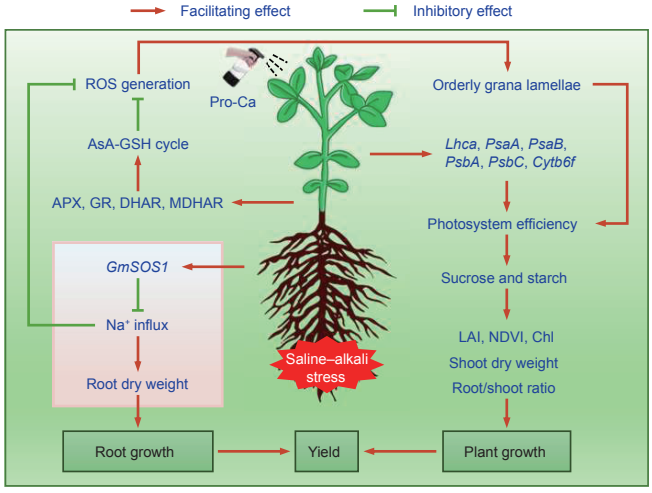

Fig. 11 A hypothetical regulatory pathway of exogenous prohexadione-calcium (Pro-Ca) mediated saline–alkali tolerance in soybean seedlings. ROS, reactive oxygen species; AsA–GSH, ascorbate–glutathione; APX, ascorbate peroxidase; GR, glutathione reductase; DHAR, dehydroascorbate reductase; MDHAR, monodehydroascorbate reductase; LAI, leaf area index; NDVI, normalized difference vegetation index; Chl, chlorophyll.

5. Conclusion

Foliar application of 100 mg L^{-1} Pro-Ca under saline–alkali stress maintained the biomembrane system by reducing Na^+ influx and reactivating the AsA–GSH cycle. Moreover, the reduction in L_s and the increase in PSII electron transport efficiency induced by Pro-Ca treatment increased P_n and productivity. This indicates that Pro-Ca for foliar applied can be an effective strategy for mitigating saline–alkali stress during soybean production in saline–alkali soils. This study provides theoretical evidence that Pro-Ca improves the tolerance of soybean seedlings to saline–alkali stress.

Acknowledgements

This work was supported by the National Natural Science Foundation of China (318576) and the Guangdong Postgraduate Education Innovation Project, China (2022XSLT036).

Declaration of competing interest

The authors declare that they have no conflict of interest.

Declaration of generative AI and AI-assisted technologies in the writing process

The authors declare that they did not use AI in the preparation and writing of this manuscript.

Appendices associated with this paper are available at https://doi.org/10.1016/j.jia.2025.04.005

References

Aghdam M S. 2013. Mitigation of postharvest chilling injury in tomato fruit by prohexadione calcium. *Journal of Food Science and Technology-Mysore*, **50**, 1029–1033.

Ahmad P, Ahanger M A, Egamberdieva D, Alam P, Alyemeni M N, Ashraf M. 2018. Modification of osmolytes and antioxidant enzymes by 24-epibrassinolide in chickpea seedlings under mercury (Hg) toxicity. *Journal of Plant Growth Regulation*, **37**, 3093–3322.

Akram S, Siddiqui M N, Hussain B M N, Al Bari M A, Mostofa M G, Hossain M A, Tran L S P. 2017. Exogenous glutathione modulates salinity tolerance of soybean [*Glycine max* (L.) Merrill] at reproductive stage. *Journal of Plant Growth Regulation*, **36**, 877–888.

Alam P, Albalawi T H, Altalayan F H, Bakht M A, Ahanger M A, Raja V, Ashraf M, Ahmad P. 2019. 24-Epibrassinolide (EBR) confers tolerance against NaCl stress in soybean plants by up-regulating antioxidant system, ascorbate-glutathione cycle, and glyoxalase system. *Biomolecules*, **9**, 640.

Bae N, Shim S H, Alavilli H, Do H, Park M, Lee D W, Lee J H, Lee H Y S, Li X Z, Lee C H, Jeon J S, Lee B H. 2024. Enhanced salt stress tolerance in plants without growth penalty through increased photosynthesis activity by plastocyanin from Antarctic moss. *Plant Journal*, **121**, e17168.

Becker T B, Schiavon A V, Delazeri E E, Barreto C F, Correa Antunes L E. 2020. Productive behavior of strawberry from potted seedlings produced with application of prohexadione calcium in soilless cultivation. *Emirates Journal of Food and Agriculture*, **32**, 309–318.

Bekheta M A, Abdelhamid M T, El-Morsi A A. 2009. Physiological response of *Vicia faba* to prohexadione-calcium under saline conditions. *Planta Daninha*, **27**, 769–779.

Bukhat S, Imran A, Javaid S, Shahid M, Majeed A, Naqqash T. 2020. Communication of plants with microbial world: Exploring the regulatory networks for PGPR mediated defense signaling. *Microbiological Research*, **238**, 126486.

Cheng C, Liu Y M, Liu X, An J, Jiang L, Yu B J. 2019. Recretohalophyte *Tamarix TrSOS1* confers higher salt tolerance to transgenic plants and yeast than glycophyte soybean *GmSOS1*. *Environmental and*

Experimental Botany, **165**, 196–207.
Davletova S, Rizhsky L, Liang H J, Zhong S Q, Oliver D J, Coutu J, Shulaev V, Schlauch K, Mittler R. 2005. Cytosolic ascorbate peroxidase 1 is a central component of the reactive oxygen gene network of *Arabidopsis*. *Plant Cell*, **17**, 268–281.
Deng P, Khan A, Zhou H, Lu X T, Zhao H M, Du Y W, Wang Y X, Feng N J, Zheng D F. 2024. Application of prohexadione-calcium priming affects *Brassica napus* L. seedlings by regulating morph-physiological characteristics under salt stress. *PeerJ*, **12**, e17312.
Deng R, Li Y, Feng N J, Zheng D F, Du Y W, Khan A, Xue Y B, Zhang J Q, Feng Y N. 2024. Integrative analyses reveal the physiological and molecular role of prohexadione calcium in regulating salt tolerance in rice. *International Journal of Molecular Sciences*, **25**, 9124.
Desneux N, Decourtye A, Delpuech J M. 2007. The sublethal effects of pesticides on beneficial arthropods. *Annual Review of Entomology*, **52**, 81–106.
Du B, Haensch R, Alfarraj S, Rennenberg H. 2024. Strategies of plants to overcome abiotic and biotic stresses. *Biological Reviews*, **99**, 1524–1536.
Duan Y J, Wang X X, Jiao Y, Liu Y Y, Li Y, Song Y Z, Wang L, Tong X H, Jiang Y, Wang S D, Wang S. 2024. Elucidating the role of exogenous melatonin in mitigating alkaline stress in soybeans across different growth stages: A transcriptomic and metabolomic approach. *BMC Plant Biology*, **24**, 380.
Estaji A, Niknam F. 2020. Foliar salicylic acid spraying effect' on growth, seed oil content, and physiology of drought-stressed *Silybum marianum* L. plant. *Agricultural Water Management*, **234**, 106116.
Fan Y, Shen W Y, Vanessa P, Cheng F Q. 2021. Synergistic effect of Si and K in improving the growth, ion distribution and partitioning of *Lolium perenne* L. under saline–alkali stress. *Journal of Integrative Agriculture*, **20**, 1660–1673.
Feng N J, Yu M L, Li Y, Jin D, Zheng D F. 2021. Prohexadione-calcium alleviates saline-alkali stress in soybean seedlings by improving the photosynthesis and up-regulating antioxidant defense. *Ecotoxicology and Environmental Safety*, **220**, 112369.
Gadelha C G, Coutinho Í A C, Pinheiro S K D P, Miguel E D C, Carvalho H H D, Lopes L D S, Gomes-Filho E. 2021. Sodium uptake and transport regulation, and photosynthetic efficiency maintenance as the basis of differential salt tolerance in rice cultivars. *Environmental and Experimental Botany*, **192**, 104654.
Großkinsky D K, Svensgaard J, Christensen S, Roitsch T. 2015. Plant phenomics and the need for physiological phenotyping across scales to narrow the genotype-to-phenotype knowledge gap. *Journal of Experimental Botany*, **66**, 5429–5440.
Guo R, Yang Z Z, Li F, Yan C R, Zhong X L, Liu Q, Xia X, Li H R, Zhao L. 2015. Comparative metabolic responses and adaptive strategies of wheat (*Triticum aestivum*) to salt and alkali stress. *BMC Plant Biology*, **15**, 170.
Gupta P, Srivastava S, Seth C S. 2017. 24-Epibrassinolide and sodium nitroprusside alleviate the salinity stress in *Brassica juncea* L. cv. Varuna through cross talk among proline, nitrogen metabolism and abscisic acid. *Plant and Soil*, **411**, 483−498.
Hasanuzzaman M, Bhuyan M H M B, Anee T I, Parvin K, Nahar K, Mahmud J A, Fujita M. 2019. Regulation of ascorbate-glutathione pathway in mitigating oxidative damage in plants under abiotic stress. *Antioxidants*, **8**, 384.
Hasanuzzaman M, Bhuyan M H M B, Zulfiqar F, Raza A, Mohsin S M, Al Mahmud J, Fujita M, Fotopoulos V. 2020. Reactive oxygen species and antioxidant defense in plants under abiotic stress: revisiting the crucial role of a universal defense regulator. *Antioxidants*, **9**, 681.
Hassani A, Azapagic A, Shokri N. 2021. Global predictions of primary soil salinization under changing climate in the 21st century. *Nature Communications*, **12**, 1–17.
Hu E M, Liu M, Zhou R, Jiang F L, Sun M T, Wen J Q, Zhu Z H, Wu Z. 2021. Relationship between melatonin and abscisic acid in response to salt stress of tomato. *Scientia Horticulturae*, **285**, 110176.
Jiang K, Guo H W, Zhai J X. 2023. Interplay of phytohormones and epigenetic regulation: A recipe for plant development and plasticity. *Journal of Integrative Plant Biology*, **65**, 381–398.
Li Y, Zhou H, Feng N J, Zheng D F, Ma G H, Feng S J, Liu M L, Yu M L, Huang X X, Huang A Q. 2023. Physiological and transcriptome analysis reveals that prohexadione-calcium promotes rice seedling's development under salt stress by regulating antioxidant processes and photosynthesis. *PLoS ONE*, **18**, e0286505.
Liu J, Shabala S, Shabala L, Zhou M X, Meinke H, Venkataraman G, Chen Z H, Zeng F R, Zhao Q Z. 2019. Tissue-specific regulation of Na^+ and K^+ transporters explains genotypic differences in salinity stress tolerance in rice. *Frontiers in Plant Science*, **10**, 1361.
Liu M L, Feng N J, Zheng D F, Zhang R J. 2024. Prohexadione calcium and gibberellin improve osmoregulation, antioxidant response and ion homeostasis to alleviate NaCl stress in rice seedlings. *Agronomy*, **14**, 1318.
Lu C X, Li L Y, Liu X L, Chen M, Wan S B, Li G W. 2023. Salt stress inhibits photosynthesis and destroys chloroplast structure by downregulating chloroplast development-related genes in *Robinia pseudoacacia* seedlings. *Plants*, **12**, 1283.
Luo B, Wang C, Wang X D, Zhang H, Zhou Y A, Wang W S, Song P. 2021. Changes in photosynthesis and chlorophyll fluorescence in two soybean (*Glycine max*) varieties under NaCl stress. *International Journal of Agricultural and Biological Engineering*, **14**, 76–82.
Mehler A H. 1951. Studies on reactions of illuminated chloroplasts: I. Mechanism of the reduction of oxygen and other hill reagents. *Archives of Biochemistry and Biophysics*, **33**, 65–77.
Mehmood S, Ahmed W, Ikram M, Imtiaz M, Mahmood S, Tu S X, Chen D Y. 2020. Chitosan modified biochar increases soybean (*Glycine max* L.) resistance to salt-stress by augmenting root morphology, antioxidant defense mechanisms and the expression of stress-responsive genes. *Plants*, **9**, 1173.
Miranda R D S, Gomes-Filho E, Prisco J T, Alvarez-Pizarro J C. 2016. Ammonium improves tolerance to salinity stress in *Sorghum bicolor* plants. *Plant Growth Regulation*, **78**, 121–131.
Mittler R. 2017. ROS are good. *Trends in Plant Science*, **22**, 11–19.
Mittler R, Zandalinas S I, Fichman Y, Van Breusegem F. 2022. Reactive oxygen species signalling in plant stress responses. *Nature Reviews Molecular Cell Biology*, **23**, 663–679.
Nakayama I, Kamiya Y, Kobayashi M, Abe H, Sakurai A. 1990. Effects of a plant-growth regulator, prohexadione, on the biosynthesis of gibberellins in cell-free systems derived from immature seeds. *Plant and Cell Physiology*, **31**, 1183–1190.
Parida A K, Jha B. 2013. Inductive responses of some organic metabolites for osmotic homeostasis in peanut (*Arachis hypogaea* L.) seedlings during salt stress. *Acta Physiologiae Plantarum*, **35**, 2821–2832.
Peña-Calzada K, Olivera-Viciedo D, Calero-Hurtado A, Prado R D M, Habermann E, Tenesaca L F L, Ajila G, de Oliveira R, Rodríguez J C, Gratão P L. 2023. Silicon mitigates the negative impacts of salt stress in soybean plants. *Journal of the Science of Food and Agriculture*, **103**, 4360–4370.
Rademacher W. 2015. Plant growth regulators: Backgrounds and uses in plant production. *Journal of Plant Growth Regulation*, **34**, 845–872.
Raja V, Majeed U, Kang H, Andrabi K I, John R. 2017. Abiotic stress: Interplay between ROS, hormones and MAPKs. *Environmental and Experimental Botany*, **137**, 142–157.
Rasool S, Ahmad A, Siddiqi T O, Ahmad P. 2013. Changes in growth, lipid peroxidation and some key antioxidant enzymes in chickpea genotypes under salt stress. *Acta Physiologiae Plantarum*, **35**, 1039–1050.
Salesse-Smith C E, Wang Y, Long S P. 2025. Increasing Rubisco as a simple means to enhance photosynthesis and productivity now without lowering nitrogen use efficiency. *New Phytologist*, **245**, 951–965.
Sharma A, Thakur S, Kumar V, Kanwar M K, Kesavan A K, Thukral A K, Bhardwaj R, Alam P, Ahmad P. 2016. Pre-sowing seed treatment with 24-epibrassinolide ameliorates pesticide stress in *Brassica juncea* L. through the modulation of stress markers. *Frontiers in Plant Science*, **7**, 1569.
Stirbet A, Govindjee. 2011. On the relation between the Kautsky effect (chlorophyll *a* fluorescence induction) and Photosystem II: Basics and applications of the OJIP fluorescence transient. *Journal of Photochemistry and Photobiology* (B: Biology), **104**, 236–257.
Sun T J, Fan L, Yang J, Cao R Z, Yang C Y, Zhang J, Wang D M. 2019. A *Glycine max* sodium/hydrogen exchanger enhances salt tolerance through maintaining higher Na^+ efflux rate and K^+/Na^+ ratio in *Arabidopsis*. *BMC Plant Biology*, **19**, 469.
Sun Z W, Ren L K, Fan J W, Li Q, Wang K J, Guo M M, Wang L, Li J, Zhang G X, Yang Z Y, Chen F, Li X N. 2016. Salt response of photosynthetic electron transport system in wheat cultivars with

contrasting tolerance. *Plant Soil and Environment*, **62**, 515–521.
Tang C N, Xie J M, Lv J, Li J, Zhang J, Wang C, Liang G P. 2021. Alleviating damage of photosystem and oxidative stress from chilling stress with exogenous zeaxanthin in pepper (*Capsicum annuum* L.) seedlings. *Plant Physiology and Biochemistry*, **162**, 395–409.
Tripodi P, Vincenzo C, Venezia A, Cocozza A, Pane C. 2024. Precision phenotyping of wild rocket (*Diplotaxis tenuifolia*) to determine morpho-physiological responses under increasing drought stress levels using the PlantEye multispectral 3D system. *Horticulturae*, **10**, 496.
Wang P T, Liu W C, Han C, Wang S T, Bai M Y, Song C P. 2024. Reactive oxygen species: Multidimensional regulators of plant adaptation to abiotic stress and development. *Journal of Integrative Plant Biology*, **66**, 330–367.
Wang S C, Ma L, Xu Y, Wang Y, Zhu N Y, Liu J Z, Dolfing J, Kerr P, Wu Y H. 2020. The unexpected concentration-dependent response of periphytic biofilm during indole acetic acid removal. *Bioresource Technology*, **303**, 122922.
Wang Y, Wang J C, Guo D D, Zhang H B, Che Y H, Li Y Y, Tian B, Wang Z H, Sun G Y, Zhang H H. 2021. Physiological and comparative transcriptome analysis of leaf response and physiological adaption to saline alkali stress across pH values in alfalfa (*Medicago sativa*). *Plant Physiology and Biochemistry*, **167**, 140–152.
Wani A S, Hayat S, Ahmad A, Tahir I. 2017. Efficacy of brassinosteroid analogues in the mitigation of toxic effects of salt stress in *Brassica juncea* plants. *Journal of Environmental Biology*, **38**, 27–36.
Waszczak C, Carmody M, Kangasjärvi J. 2018. Reactive oxygen species in plant signaling. *Annual Review of Plant Biology*, **69**, 209–236.
Xin L, Tang M S, Zhang L, Huang W X, Wang X P, Gao Y. 2024. Effects of saline-fresh water rotation irrigation on photosynthetic characteristics and leaf ultrastructure of tomato plants in a greenhouse. *Agricultural Water Management*, **292**, 108671.
Xu C, Li Q, Liu X L, Wang H J, Liang X H, Ling F L, Wu Z H, Zhang Z A, Chen Z Y. 2019. Effects of nitrogen supply level on photosynthesis and chlorophyll fluorescence characteristics of rice under salt stress. *Emirates Journal of Food and Agriculture*, **31**, 741–751.
Yang F, Feng L Y, Liu Q L, Wu X L, Fan Y F, Raza M A, Cheng Y J, Chen J X, Wang X C, Yong T W, Liu W G, Liu J, Du J B, Shu K, Yang W Y. 2018. Effect of interactions between light intensity and red-to-far-red ratio on the photosynthesis of soybean leaves under shade condition. *Environmental and Experimental Botany*, **150**, 79–87.
Yi X P, Hargett S R, Liu H J, Frankel L K, Bricker T M. 2007. The PsbP protein is required for photosystem II complex assembly/stability and photoautotrophy in *Arabidopsis thaliana*. *Journal of Biological Chemistry*, **282**, 24833–24841.
Zhang B S, Liu Z, Zhou R N, Cheng P, Li H B, Wang Z Y, Liu Y, Li M Y, Zhao Z Q, Hu Z B, Chen Q S, Wu X X, Zhao Y. 2023. Genome-wide analysis of soybean *DnaJA*-family genes and functional characterization of *GmDnaJA6* responses to saline and alkaline stress. *Crop Journal*, **11**, 1230–1241.
Zhang M H, Cao J F, Zhang T X, Xu T, Yang L Y, Li X Y, Ji F D, Gao Y X, Ali S, Zhang Q Z, Zhu J H, Xie L N. 2022. A putative plasma membrane Na^+/H^+ antiporter GmSOS1 is critical for salt stress tolerance in *Glycine max*. *Frontiers in Plant Science*, **13**, 870695.
Zhang Y, Zhou X J, Dong Y T, Zhang F, He Q L, Chen J H, Zhu S J, Zhao T L. 2021. Seed priming with melatonin improves salt tolerance in cotton through regulating photosynthesis, scavenging reactive oxygen species and coordinating with phytohormone signal pathways. *Industrial Crops and Products*, **169**, 113671.
Zhang Z Z, He K N, Zhang T, Tang D, Li R J, Jia S F. 2019. Physiological responses of Goji berry (*Lycium barbarum* L.) to saline-alkaline soil from Qinghai region, China. *Scientific Reports*, **9**, 12057.
Zhao Q, Liu L, Wei Z H, Bai Q Y, Zhao C A, Zhang S H, Pan J L, Yu J X, Zhang S, Wei J. 2024. Gamma-aminobutyric acid (GABA) improves salinity stress tolerance in soybean seedlings by modulating their mineral nutrition, osmolyte contents, and ascorbate-glutathione cycle. *BMC Plant Biology*, **24**, 365.
Zhao Q, Shen W Z, Gu Y H, Hu J C, Ma Y, Zhang X L, Du Y L, Zhang Y X, Du J D. 2023. Exogenous melatonin mitigates saline-alkali stress by decreasing DNA oxidative damage and enhancing photosynthetic carbon metabolism in soybean (*Glycine max* [L.] Merr.) leaves. *Physiologia Plantarum*, **175**, e13983.
Zhu L X, Sun H C, Wang R R, Guo C C, Liu L T, Zhang Y J, Zhang K, Bai Z Y, Li A C, Zhu J H, Li C D. 2024. Exogenous melatonin improves cotton yield under drought stress by enhancing root development and reducing root damage. *Journal of Integrative Agriculture*, **23**, 3387–3405.
Zhu X C, Liu S Q, Sun L Y, Song F B, Liu F L, Li X G. 2018. Cold tolerance of photosynthetic electron transport system is enhanced in wheat plants grown under elevated CO_2. *Frontiers in Plant Science*, **9**, 933.